

Source attributions of radiative forcing by regions, sectors, and climate forcers

Xuanming Su^{1*}, Kaoru Tachiiri^{1,2}, Katsumasa Tanaka^{2,3}, Michio Watanabe¹ & Michio Kawamiya¹

¹Research Institute for Global Change / Research Center for Environmental Modeling and Application / Earth System Model Development and Application Group, Japan Agency for Marine-Earth Science and Technology (JAMSTEC), Yokohama, Japan

²Center for Global Environmental Research, National Institute for Environmental Studies (NIES), Tsukuba, Japan

³Laboratoire des Sciences du Climat et de l'Environnement (LSCE), Commissariat à l'Énergie atomique et aux Énergies alternatives (CEA), Gif-sur-Yvette, France

E-mail: *suxuanming@jamstec.go.jp

Abstract. It is important to understand how the emissions of different regions, sectors, or climate forcers play a role on pathways toward the Paris Agreement temperature targets. There are however methodological challenges for attributing individual contributions due to complexities associated with a variety of climate forcers affecting the climate system on different spatial and temporal scales. Here, we use the latest historical and future emissions data for a comprehensive set of climate forcers as well as land-use datasets and apply the normalized marginal approach to quantify the forcing contributions of regions, sectors and forcing agents toward the 2 °C and 1.5 °C targets. We show that most of the worldwide regions and sectors need to maintain forcing levels not higher than present levels to attain the 1.5 °C target of the Paris Agreement, while slightly higher future forcing levels than present levels are allowed for the 2 °C target. Our results illustrate the importance of negative CO₂ emissions, which contribute $-0.75 \pm 0.44 \text{ Wm}^{-2}$ and $-0.42 \pm 0.27 \text{ Wm}^{-2}$ to the 2 °C and 1.5 °C targets. Less negative forcings, or more positive forcings are also identified for the land-use albedo for the 2 °C and 1.5 °C scenarios compared to existing studies.

1. Introduction

The Paris Agreement has set goals to limit the global average temperature increase to well below 2 °C and to pursue efforts to limit the temperature increase to 1.5 °C above the preindustrial level. The Paris Agreement goals can be translated into the required levels of greenhouse gas (GHG) emission reductions [1–6] for practical implementation purposes, through calculations of the radiative forcings resulting from various emission sources. Attaining the radiative forcing of 2.6 Wm⁻² and 1.9 Wm⁻² are known to be largely consistent with achieving the 2 °C and 1.5 °C climate goals, respectively, at an approximately 66% probability [1, 3, 7–10]. Here we use the radiative forcing as a benchmark and assess how individual regions, sectors, and climate forcers can contribute to achieving the Paris Agreement temperature targets based on a latest set of historical and future emission data. Such source attribution cannot be done from emissions data alone because a variety of climate forcers affect the climate system on different temporal and spatial scales in nonlinear ways, requiring dedicated methodologies like the one presented here. Attributing forcing at the levels of regions, sectors, or climate forcers provides a basis for considering the principle of common but differentiated responsibilities contained in the 1992 United Nations Framework Convention on Climate Change (UNFCCC).

We identified two issues associated with previous attribution methods. First, comprehensive regional and sectoral assessments should in principle consider a full suite of anthropogenic sources at the regional and sectoral levels, including GHGs, aerosols and pollutants, as well as land-use albedo. However, not all sources have been considered in previous studies. For example, aerosols and pollutants were not always examined [11, 12], or only a subset of aerosol species was considered (such as sulfate aerosols [13]). Also, land-use albedo were sometimes not included [11–13]. This may be due to the lack of datasets or difficulties in representing regional or sectoral forcings, but the latest datasets provide opportunities to consider a more comprehensive set of GHGs and related agents. Second, among various methods proposed, only the marginal and time-sliced methods are considered to be useful based on a satisfaction test of eight essential criteria [14, 15]. In principle, an attribution method needs to ensure additivity regarding regions and time. Implementing a non-additive method like the residual method used in [16] may introduce bias to the outcome for regions with high and low emissions. Some of the methods yield non-zero radiative forcing when a region's concentration has become zero. On the other hand, the two recommended methods are computationally expensive, especially when various sources of uncertainties are considered.

We apply the most up-to-date emissions and land-use datasets (Tables S1 to S3 and Figs. S1 to S4), which resolve regions and sectors and contain all pertinent forcing sources, including GHGs, aerosols and pollutants, and land-use albedo, as well as their associated uncertainties. Particularly we consider a range of future emissions trajectories with various socioeconomic backgrounds and climate mitigation levels [17, 18]. We combine the normalized marginal method, which is computationally less expensive than the time-sliced method [14], with a simple climate model - the Simple Climate Model

for Optimization version 2 (SCM4OPT v2.0) [19, 20]. SCM4OPT v2.0 is designed to be lightweight and suitable for performing a large number of simulations required for our study exploring uncertainties, while resolving diverse characteristics of forcing agents considered. Furthermore, based on the premise of previous studies [11, 21, 22], we make the attribution analysis more comprehensive by considering historical and future emissions and providing perspectives from regions, sectors, and climate forcers. We consider two types of uncertainties, including those due to our lack of knowledge regarding historical emissions and future projections (emission uncertainties), and those due to low confidence in understanding the climate system (climate uncertainties). With these methodological advances, we quantify the forcing contributions of regions, sectors, and climate forcers toward the Paris Agreement temperature goals.

2. Methods

We compile the emissions and land cover datasets at regional and sectoral levels and implement them to SCM4OPT v2.0 to calculate the marginal forcing effects of forcing agents at regional and sectoral levels. The relative forcing contribution of the forcing agents at regional and sectoral levels can be distinguished based on the fraction accounting for their marginal effects in total marginal effects caused by the forcing agent. The forcing contributions of the forcing agents at regional and sectoral levels can be therefore attributed. We sum up the associated individual forcings to obtain the radiative forcings resulting from regional and sectoral sources.

2.1. Emission data and uncertainties

We used historical and future emissions and land cover datasets with both regional and sectoral details. The available datasets are shown in Tables S1 to S3 and Figs. S1 to S4 [17, 18, 23–26]. We designated historical sources as those originating from 1850 to 2016, and future projections by 2100 are grouped by the forcing level at 1.9 Wm^{-2} and 2.6 Wm^{-2} , regardless of the underlying socioeconomic development or technological assumptions. We also included other scenarios with relatively lower possibilities to achieve the 2°C and 1.5°C targets, namely, forcing levels of 3.4 Wm^{-2} , 4.5 Wm^{-2} , 6.0 Wm^{-2} , 7.0 Wm^{-2} and 8.5 Wm^{-2} (Table S2). Thus, a broad range of forcings can be examined for future climate change. For the future emission datasets, 25 of them are obtained from the Asia-Pacific Integrated Model/Computable General Equilibrium (AIM/CGE) model [17], and the remaining nine are from the Integrated Assessment Modeling Consortium (IAMC) [18] (Table S2). We divided the world into eleven regions, including 1) China (CHN), 2) India (IND), 3) Japan (JPN), 4) Russia (RUS), 5) the United States of America (USA), 6) sub-Saharan Africa (AFR), 7) Europe (EUR), 8) Latin America and the Caribbean (LAM), 9) the Middle East and North Africa (MEA), 10) other areas in Asia (OAS) and 11) the rest of the world (ROW) (Table S4). For each region, twelve emitting sectors [17, 18, 23] were assessed, namely, 1) agriculture, 2) agricultural waste burning, 3) domestic and commercial housing, 4) energy, 5) industry, 6)

industrial solvents, 7) surface transportation, 8) waste treatment, 9) open forest burning, 10) open grassland burning, 11) aviation and 12) international shipping (Table S5). In addition to the twelve sectors above, 13) land-use CO₂ emissions and 14) negative CO₂ emissions, namely, through carbon capture and storage (CCS) and bioenergy with CCS (BECCS), were separately considered. We compiled the emissions from the available datasets into scenario-, region- and sector-specific emissions and used $E_{n,r,s,e}(t)$ to denote scenario (n)-, region (r)- and sector (s)-specific emissions (e , refer to the emission species) over time t . The emissions of the same forcing target originating from different Shared Socioeconomic Pathways (SSPs) and integrated assessment models (IAMs) were treated as emission uncertainties. For example, we iteratively simulated the 1.9 Wm⁻² forcing scenario by using dataset from the AIM/CGE (SSP1-1.9 and SSP2-1.9) and the IAMC (SSP1-1.9), as reported in Table S2.

2.2. Climate model and uncertainties

We used the simple climate model SCM4OPT v2.0 to generate the outputs for our analysis. The current model has been updated from the precedent in the following four respects: First, we adopted the ocean carbon cycle of Hector v1.0 [27] and applied the Diffusion Ocean Energy balance CLIMate (DOECLIM) model [28–30] to calculate the temperature change. We calibrated the carbon cycle and temperature modules based on 26 coupled atmosphere-ocean general circulation models (AOGCMs) with outputs for the carbon cycle in the Coupled Model Intercomparison Project, Phase 5 (CMIP5) (Table S6). Second, parameters associated with CH₄, N₂O and halogenated gases (a total of 37 gases, see Table S7) were tuned against the atmospheric lifetimes and radiative efficiencies in the IPCC Fifth Assessment Report (AR5) [31]. Third, we employed the simple global parameterizations described in OSCAR v2.2 [32] to estimate the radiative forcings resulting from aerosols and pollutants. The radiative forcing of short-lived climate forcers depends on the geographical location of emissions. The spatial distribution of the radiative forcing of short-lived species is different from that of long-lived species [33, 34]. However, these two effects are not considered in our analysis. Fourth, we adopted a simple parameterization scheme [32] to calculate the land-use albedo (see Eq. (67) in the supplementary materials). The equations for the climate model are listed in the supplementary materials.

We performed a robustness test over the historical period by using historical emission datasets as input and considering the climate uncertainties that were applied in this analysis. The outputs from our model are consistent with those of other models or statistical records (Figs. S5 to S8, S10 and S11). Furthermore, the likelihoods of meeting the 2°C and 1.5 °C targets of each of the forcing scenarios obtained from our model agree largely with the corresponding IPCC ranges (Fig. S12) to limit global warming to 2°C with at least 66% probability and 1.5 °C with 50% [3].

2.3. Calculation of the regional and sectoral forcings

We utilized and expanded the normalized marginal method presented in ref [14, 15, 22] to conduct our analysis. The relative forcing contribution of emission $E_{n,r,s,e}$ (Column 2 in

Table S7) to the associated radiative forcing f (Column 4 in Table S7), which is defined as $\alpha_{n,r,s,e}^f$, is proportional to the marginal effect of $E_{n,r,s,e}$ causing the radiative forcing f (see Fig. S13). To calculate $\alpha_{n,r,s,e}^f$ for each $E_{n,r,s,e}$, we performed two simulations, i.e., 1) one simulation with all emissions included in the simulation as input, to calculate the associated radiative forcing termed $F_{n,r,s,e}^{all,f}$, and 2) another simulation with the emission e reduced by $E_{n,r,s,e} \cdot \epsilon$ ($\epsilon = 0.001$) over the evaluation period, that is 1850-2100, to obtain the corresponding radiative forcing named $F_{n,r,s,e}^{\epsilon,f}$. The relative contribution $\alpha_{n,r,s,e}^f$ is obtained by:

$$\alpha_{n,r,s,e}^f = \frac{F_{n,r,s,e}^{all,f} - F_{n,r,s,e}^{\epsilon,f}}{\sum_{r,s,e} (F_{n,r,s,e}^{all,f} - F_{n,r,s,e}^{\epsilon,f})} \quad (1)$$

Therefore, the radiative forcing $F_{n,r,s,e}^f$, which is resulting from $E_{n,r,s,e}$, is isolated by:

$$F_{n,r,s,e}^f = F_{n,r,s,e}^{all,f} \cdot \alpha_{n,r,s,e}^f \quad (2)$$

To consider the relevant emission and climate uncertainties, we carried out 200 similar pairs of runs for each forcing-level-specific source $E_{n,r,s,e}$, with randomized scenarios at the same forcing level and randomized parameter sets for the climate system, and we call them as one experiment for $E_{n,r,s,e}$ (see the randomization sources of the scenarios (within each forcing level) and the climate system in Table S8). Here, the value of 200 has been tested to ensure that two decimal places of the precision level could be achieved for the mean forcing value of $F_{n,r,s,e}^f$ under different experiments.

We obtain the individual forcing agents by summing the forcings induced by all available emissions sources. Therefore, a certain forcing agent is probably a mixed effect resulting from various emissions sources. On the other hand, a particular emission may result in different kinds of radiative forcings, as indicated in Table S7. For example, black carbon (BC) can cause BC forcing, BC on snow and indirect cloud effects. A total of 5.3×10^6 runs (7.6×10^5 for each forcing level) were performed considering all forcing levels, regions, sectors and emissions. To derive the regional forcings, we applied the Monte Carlo approach ($n = 20,000$) to sum all $F_{n,r,s,e}^f$ values belonging to a given region. Here, the value of 20,000 for n was also tested to ensure the necessary precision for our analysis. The sectoral forcings are similarly obtained. An overview of all the iterations are contained in Table S8.

2.4. The probability of exceeding 2°C or 1.5°C

For each experiment, 200 sample results were acquired. Here, we assumed that the obtained temperature increase T over time t followed a normal distribution, and the cumulative distribution function was defined as:

$$F_T^t(\tau) = P^t(T \leq \tau) \quad (3)$$

We used the exceedance of Eq. (3) to obtain the probability of exceeding a specified climate target τ :

$$\overline{F}_T^t(\tau) = P^t(T > \tau) = 1 - F_T^t(\tau) \quad (4)$$

Therefore, $\overline{F}_T^t(2)$ indicates the probability of exceeding 2°C, and $\overline{F}_T^t(1.5)$ gives the probability of exceeding 1.5°C.

3. Results

3.1. Regional attributions

We performed our analysis based on the available existing scenarios, and the 2 °C or 1.5 °C results herein thus reflect the diagnosed compatible scenarios in terms of the 2 °C or 1.5 °C targets. The results reveal that the USA, China and the European Union (EU) are three major emitters, accounting for approximately 45% of all the forcings under the historical, 2 °C and 1.5 °C scenarios (see Fig. 1a). China's share increased from $12 \pm 4\%$ ($0.25 \pm 0.09 \text{ Wm}^{-2}$) by 2016 (cf. $10 \pm 4\%$ for Chinese data (1750-2010) in ref [22] with similar methods) to 2 °C's $16 \pm 3\%$ ($0.41 \pm 0.08 \text{ Wm}^{-2}$) and 1.5 °C's $17 \pm 4\%$ ($0.29 \pm 0.07 \text{ Wm}^{-2}$), while the share of the EU declined, from the historical $15 \pm 2\%$ ($0.32 \pm 0.04 \text{ Wm}^{-2}$) level to the 2 °C level of $12 \pm 2\%$ ($0.31 \pm 0.06 \text{ Wm}^{-2}$) and the 1.5 °C level of $13 \pm 3\%$ ($0.23 \pm 0.06 \text{ Wm}^{-2}$) (for the forcing values, see Fig. 2a&Fig. S14). In contrast, the share of the USA exhibited no major changes, contributing to approximately 17% of the total forcings under all three scenarios. However, the absolute values of the forcings varied, i.e., the 2 °C forcing attributed to the USA increased to $0.42 \pm 0.07 \text{ Wm}^{-2}$ from the current forcing value of $0.36 \pm 0.05 \text{ Wm}^{-2}$, while the 1.5 °C forcing value declined to $0.29 \pm 0.06 \text{ Wm}^{-2}$. Latin America and the Caribbean (as one region) also exhibited a relatively high historical share with $12 \pm 3\%$; however, the value substantially declined under both target scenarios.

CO₂, including fuel CO₂, land-use CO₂, and negative CO₂, if applicable, is the main contributor and varies across regions. Among them, China, the USA, and the Middle East and North Africa (as one region) exhibited the highest net growth forcings under the 2 °C scenario, with values of $0.08 \pm 0.14 \text{ Wm}^{-2}$, $0.07 \pm 0.13 \text{ Wm}^{-2}$ and $0.07 \pm 0.06 \text{ Wm}^{-2}$, respectively. Under the 1.5 °C scenario, the CO₂ forcings in all regions decreased. The largest decline occurred in Latin America and the Caribbean, from the historical value of $0.20 \pm 0.04 \text{ Wm}^{-2}$ to the 1.5 °C scenario value of $0.08 \pm 0.05 \text{ Wm}^{-2}$, which occurred due to the negative CO₂ emissions and the great decrease in land-use CO₂ emissions.

The non-CO₂ forcings described here refer to the forcings induced by sources other than CO₂, and these forcings also play an important role in the historical period, although they are almost adequately controlled under the 2 °C and 1.5 °C scenarios (also shown in Fig. S14). Basically, most of the regions reveal net positive non-CO₂ forcings in the historical period. Particularly in regard to Latin America and the Caribbean, the relatively high net positive non-CO₂ forcing, combined with the relatively high land-use CO₂ forcing, contributes to a comparatively large forcing share in the historical period, although the fossil-fuel forcing is relatively smaller. It is worth noting that the regions with nearly zero-sum non-CO₂ forcings contribute considerable amounts of both positive and negative forcings, such as China and

the rest of the world, in the historical period. For future non-CO₂ forcings, however, sub-Saharan Africa is found to exhibit a reasonable increase in net forcing due to its continuous development and industrialization and population growth, which requires more biomass for cooking and heating purposes, as well as changes in land cover [17, 18].

The total forcing, including the forcings that cannot be assigned to any region, increases to $2.6 \pm 0.4 \text{ Wm}^{-2}$ under the 2 °C scenario but declines to $1.8 \pm 0.4 \text{ Wm}^{-2}$ under the 1.5 °C scenario, which is lower than the current level of $2.2 \pm 0.4 \text{ Wm}^{-2}$ (Fig. 1b). All regional forcings indicate net warming effects, with positive forcing values. Forcing increases are encountered in most of the regions except in Russia, the EU, Latin America and the Caribbean, and the rest of the world under the 2 °C scenario, while the main increases still occur in two developing regions, namely, China and the Middle East and North Africa under the 1.5 °C scenario (Fig. 2a&Fig. S14). Here, the forcing increases in the Middle East and North Africa can mostly be attributed to fossil-fuel CO₂, sulfate, cloud effects, and land-use albedo, probably due to industry and energy supply expansions as well as due to the expected reforestation in this area [17]. The regional nonattributable forcings in the historical period also reveal warming effects. These forcings are later notably suppressed under both the 2 °C and 1.5 °C scenarios (Fig. 1b), and they are mainly attributed to the control of ozone-depleting substances (ODSs) under the various scenario assumptions (Fig. S1) [17, 18].

3.2. Sectoral constituents

The regional effects are further separated into their sectoral constituents to assess how future changes occur (Fig. 2a). First, for the developed regions, relatively large increases are observed in both industrial and housing sectors under the 2 °C scenario. In regard to energy, the gross forcings related to the USA and EU are considerably high under the 2 °C scenario. However, if combined with the negative CO₂ emissions, the energy forcings decrease to $0.12 \pm 0.11 \text{ Wm}^{-2}$ and $0.07 \pm 0.08 \text{ Wm}^{-2}$ for the USA and EU, respectively, which are lower than the current levels. Second, among the developing regions, China's industry exhibits the most significant forcing increase, with a value of $0.14 \pm 0.07 \text{ Wm}^{-2}$ under the 2 °C scenario. In addition to the industrial sector, prominent increases are found in the agricultural sector, such as in sub-Saharan Africa, and the forcing induced by the agricultural sector increases by $0.09 \pm 0.03 \text{ Wm}^{-2}$ under the 2 °C scenario. In addition, the land-use CO₂ forcings are alleviated to varying degrees in all regions under the 2 °C scenario. Under the 1.5 °C scenario, most of the regions still demonstrate increased forcings in the industrial sector, while in the developed regions, the forcings in the industrial sector decrease. Furthermore, both the negative and land-use CO₂ emissions could result in extensive forcing abatement from the current levels in the developing regions under the 1.5 °C scenario.

Globally, in certain sectors, as shown in Fig. 2b, the forcings still increase to certain levels under the 2 °C scenario, except for the land-use CO₂ and other sources that are responsible for the main emissions of aerosols and pollutants, such as waste treatment, agricultural waste burning, forest burning and grass burning. However, under the 1.5 °C scenario, except for the energy sector and land-use albedo, only a small amount of the forcings is found to increase

in the major emitting sectors, such as domestic and commercial housing, industrial sector, aviation and international shipping. In addition, as also indicated in the analysis of the individual forcing agents below, the negative CO₂ emissions remove a considerable amount of forcings from the energy sector under the 1.5 °C scenario, and the net forcing level in the energy sector is lower than the current energy sector level. This result implies that to attain the 1.5 °C target, efforts need to be implemented to maintain the sectoral forcings below or equal to the current levels.

3.3. Individual forcing agents

Fig. 3a shows the individual forcing agents for each sectoral source. Fossil-fuel CO₂ dominates the forcings in the housing, energy, industrial and transport sectors, particularly under the 2°C and 1.5 °C scenarios when the other GHGs and aerosols and pollutants are substantially removed (Figs. S1 to S3) and the resulting impacts are therefore greatly reduced.

Among them, first, the negative CO₂ emissions can eliminate considerable amounts of forcings. For example, $-0.75 \pm 0.44 \text{ Wm}^{-2}$ and $-0.42 \pm 0.27 \text{ Wm}^{-2}$ are attributed to the negative CO₂ emissions under the 2 °C and 1.5 °C scenarios, respectively, (Fig. 3a). It is interesting to note that the reduced amount of the absolute forcing under the 2 °C scenario is even larger than that under the 1.5 °C scenario. This finding explains the feasibility of the relatively weaker climate policies adopted under the 2 °C scenario, leading to higher gross fossil CO₂ emissions. However, a fair amount of fossil CO₂ emissions is removed in the later period when the costs related to the negative CO₂ emissions are more reasonable. Under the 1.5 °C scenario, stronger strategies are implemented after the early period. Thus, the gross fossil CO₂ emissions are relatively lower, and the required negative CO₂ emissions do not need to be as high [17]. Here, the general trend can be simply interpreted as that of emit more but reduce more. Moreover, if considering the negative CO₂ emissions, the net forcings are actually lower than the current levels in the energy sector under both the 2 °C (0.42 Wm^{-2}) and the 1.5 °C (0.31 Wm^{-2}) scenarios, although gross increases are prominent (Fig. 3a).

Second, in regard to agriculture, the major sources are CH₄ and N₂O. A considerable amount of the forcings induced by CH₄ and N₂O still remains under the 2 °C and 1.5 °C scenarios (Fig. 3a), due to difficulties in reducing the CH₄ and N₂O emissions from agriculture [17, 18] and their relatively long lifetimes, namely, 12.4 years for CH₄ and 121 years for N₂O (see Table 8.A.1 in ref [8]).

Third, the land-use albedo currently exhibits a cooling effect of $-0.16 \pm 0.03 \text{ Wm}^{-2}$. However, the land-use albedo may reveal warming effects in the future, at $0.03 \pm 0.08 \text{ Wm}^{-2}$ under the 2 °C scenario and $0.05 \pm 0.13 \text{ Wm}^{-2}$ under the 1.5 °C scenario (Fig. 3b). The forest cover is expected to increase under the 2 °C and 1.5 °C scenarios (Fig. S4), which will lower the surface albedo and reflect less of the incoming solar radiation, which in turn will generate lower negative forcings, or more positive forcings, while the current deforestation causes a negative forcing [35]. Therefore, to achieve the set climate goals, more forcings need to be reduced from other sources to compensate for this effect. Here, the land-use albedo is estimated by a simple parameterization scheme [32, 36] constrained by future land

cover changes (see Methods), and the results reveal lower negative forcings, or more positive forcings, than those by the other estimations (Fig. S9).

3.4. Attributions under the high-emission scenarios

All potential projected scenarios, including those forcings higher than the 2°C and 1.5 °C forcings, are shown in Fig. 4a (for the regional contributions) and Fig. 4b (for the sectoral forcings). We translate the forcing levels into probabilities of exceeding 2°C or 1.5°C to demonstrate the likelihood of achieving the climate goals under such conditions. Basically, China, the USA and the EU are still the three major contributors to climate change when high forcings are applied. For example, under the high-forcing scenarios, China may account for approximately 1.1 Wm⁻², albeit with greater uncertainty, the USA accounts for approximately 0.9 Wm⁻², and the EU accounts for approximately 0.6 Wm⁻². All other regions exhibit relatively lower but still significant radiative forcings under the same circumstances, except Japan, where the forcing levels do not greatly change even under the high-forcing scenarios. Sectorally, the energy sector may contribute the highest forcings given its high emissions, up to 3.8 Wm⁻², followed by the industry (up to 1.4 Wm⁻²) and transport (up to 1.1 Wm⁻²), as well as land-use CO₂ (up to 0.8 Wm⁻²). Lower or no negative CO₂ emissions (Fig. S1), relatively fewer nuclear and renewable energy sources (for example, solar and wind), and more fossil-fueled energy use could bring about extremely high climate-related emissions in the energy sector [17, 18, 37, 38]; hence, high forcings are produced. All sectors reveal high radiative forcing values except for open burning, which remains relatively stable, under the assumed high-forcing scenarios (Fig. 4b).

4. Discussion

In this study, we applied a simple climate model, SCM4OPT v2.0, to determine the forcing contributions of regions, sectors and climate forcers based on available historical and future projection emissions and land-use datasets. This study provides an IAM-based assessment from a forcing perspective at the sectoral and regional levels. The radiative forcings, including the forcings resulting from the various sources of GHGs, aerosols and pollutants, and land-use albedo, are distinguished among the different regions and sectors. The outputs here can be used to inform policy-makers of the relative importance of the forcing levels resulting from different regional or sectoral sources.

The results are interpreted with certain caveats and limitations. First, we analyze emission datasets that contain regional and sectoral information, while global-scale datasets are not included. Therefore, our analysis only reflects limited uncertainties that are derived from the available emission estimates. Thus, the analysis here is merely considered as an IAM-based evaluation of the potential future climate, especially under the 2°C and 1.5 °C scenarios. Second, the outcome of this study is contingent on the set of selected scenarios used, which are treated equally likely. However, the distribution of total range of future emissions does not necessarily present equal probabilities [39] (Fig. S15). We consider a

further update for this analysis when the probabilistic emission scenarios are available.

The results showed that the 1.5 °C target requires most regions and sectors to maintain their forcings not higher than the current levels, while slightly higher future forcing levels than present levels are allowed for the 2 °C target. The results here can be used to assess the gap between the current and targeted climate levels for both regions and sectors in terms of the radiative forcing. Furthermore, we found that the negative CO₂ forcing is projected to contribute $-0.75 \pm 0.44 \text{ Wm}^{-2}$ and $-0.42 \pm 0.27 \text{ Wm}^{-2}$ under the 2 °C and 1.5 °C scenarios, respectively. Our analysis illustrates the importance of the negative CO₂ emissions in achieving the climate targets from the perspective of the radiative forcing. By using a new land-use forcing parameterization, we further found that less negative forcings, or more positive forcings, for the land-use albedo for the 2 °C and 1.5 °C scenarios than those from existing studies. A comprehensive consideration of the available forcing sources is important for the climate change assessment.

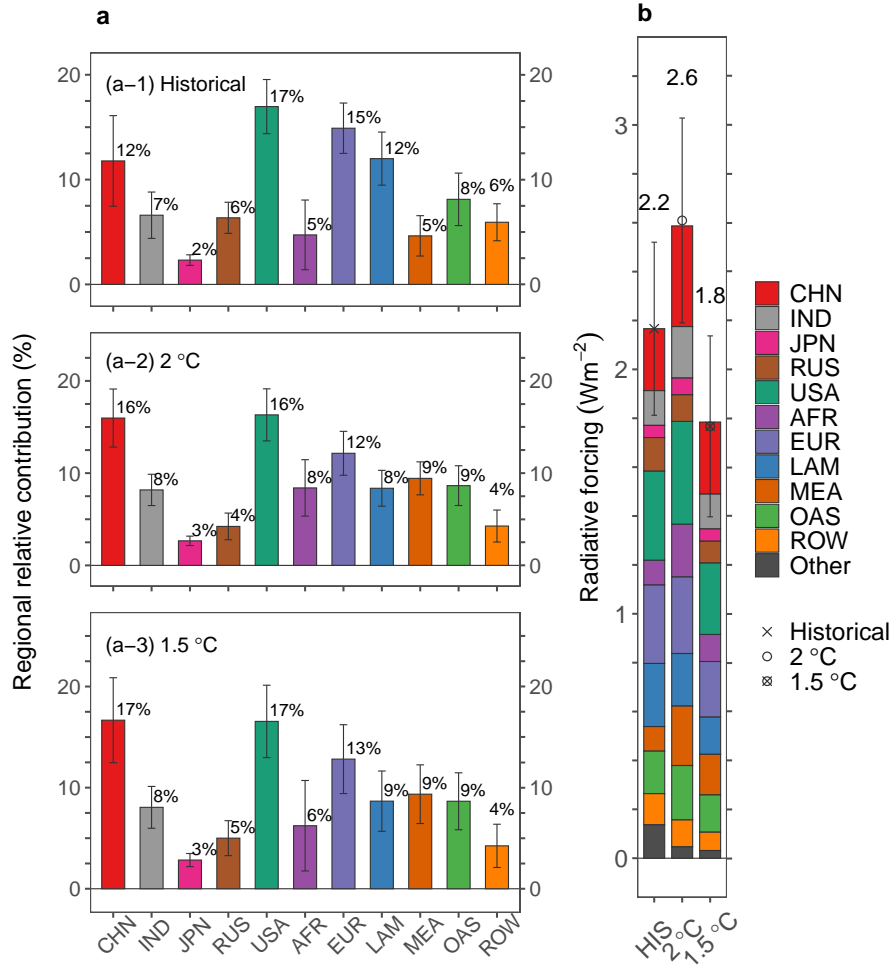


Figure 1. Reginal contributions to climate change. a, Regional relative contributions to climate change. The regional relative contributions are derived from the elementwise ratio of the regional forcings to the total forcings via the methods described in ref [22]. Note that the sum of the mean percentages of all regions is not equal to 100% since regional nonattributable forcings occur (see Fig. 1b). b, The world total forcings are divided into regional forcings. The value on top of the bar indicates the mean value of the total radiative forcing, and the error bar indicates the associated uncertainty resulting from the world ensemble. The other forcings in Fig. b are the regional nonattributable climate forcers, including the international shipments of 0.01 ± 0.03 , 0.06 ± 0.02 , and 0.05 ± 0.03 Wm^{-2} and part of the ozone-depleting substances (ODSs) of 0.23 ± 0.05 , 0.07 ± 0.03 , and 0.07 ± 0.03 Wm^{-2} (for the regional nonattributable forcings, see Table S7), under the historical, 2 °C and 1.5 °C scenarios, as well as mineral dust (Fig. S6) and the effects of solar irradiance and volcanic activity (Fig. S8). The probabilities of reaching the 2 °C and 1.5 °C targets here are 56% and 61%, respectively (see Fig. 4). All uncertainties are represented as one standard deviation. CHN, China; IND, India; JPN, Japan; RUS, Russia; USA, United States of America; AFR, sub-Saharan Africa; EUR, Europe; LAM, Latin America and the Caribbean; MEA, Middle East and North Africa; OAS, other Asian countries; ROW, the rest of the world; Other, regional nonattributable forcings.

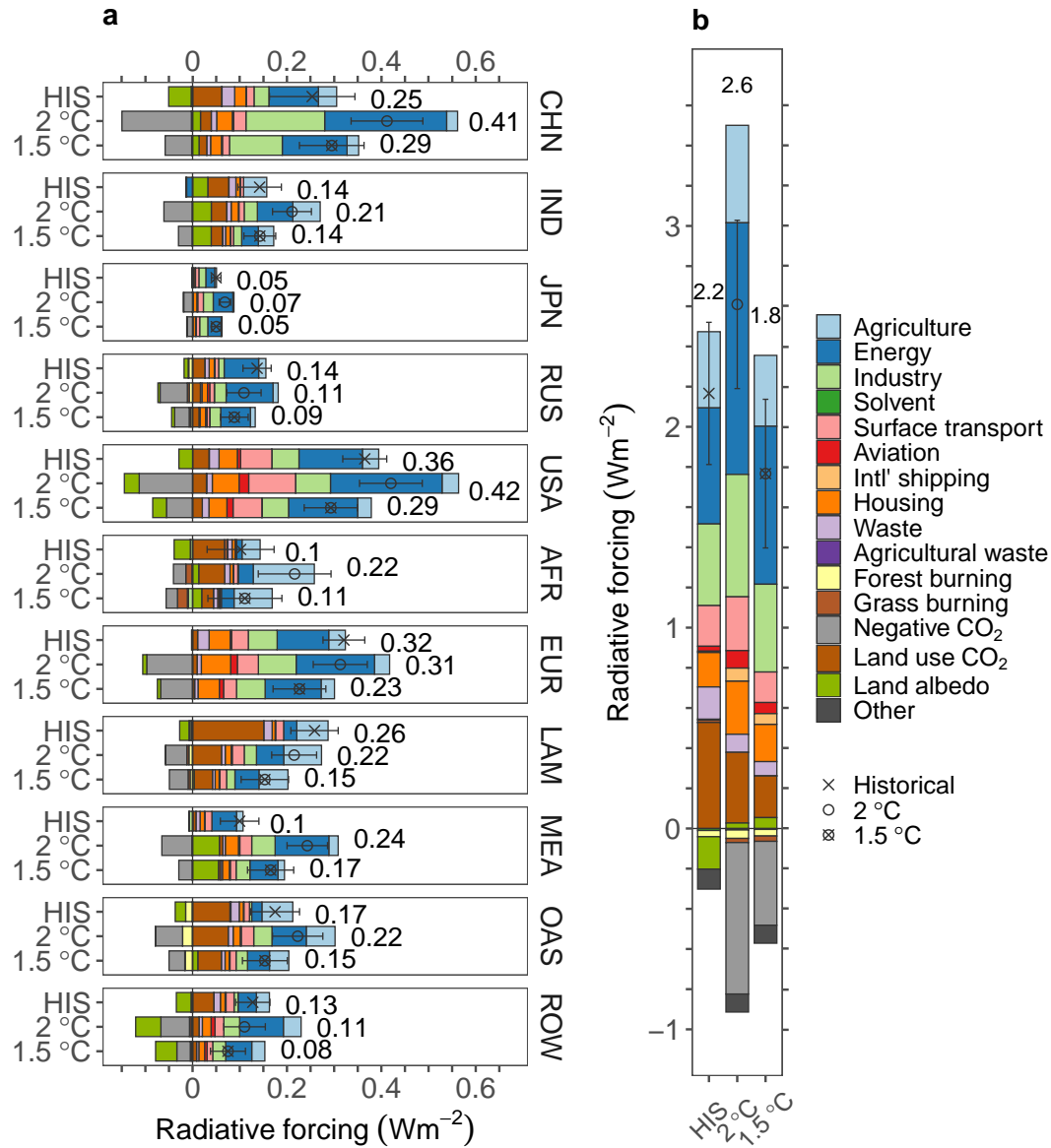


Figure 2. Sectoral contributions to climate change. a, Sectoral contributions of the eleven regions worldwide. b, The world total forcings are decomposed into sectoral forcings. The value on top of the bar indicates the mean value of the total radiative forcing, and the error bar indicates the associated uncertainty resulting from the world ensemble. The other forcings are the forcings induced by mineral dust (Fig. S6), solar irradiance and volcanic activity (Fig. S8). The probabilities of reaching the 2 °C and 1.5 °C targets here are 56% and 61%, respectively (see Fig. 4). All uncertainties are represented as one standard deviation.

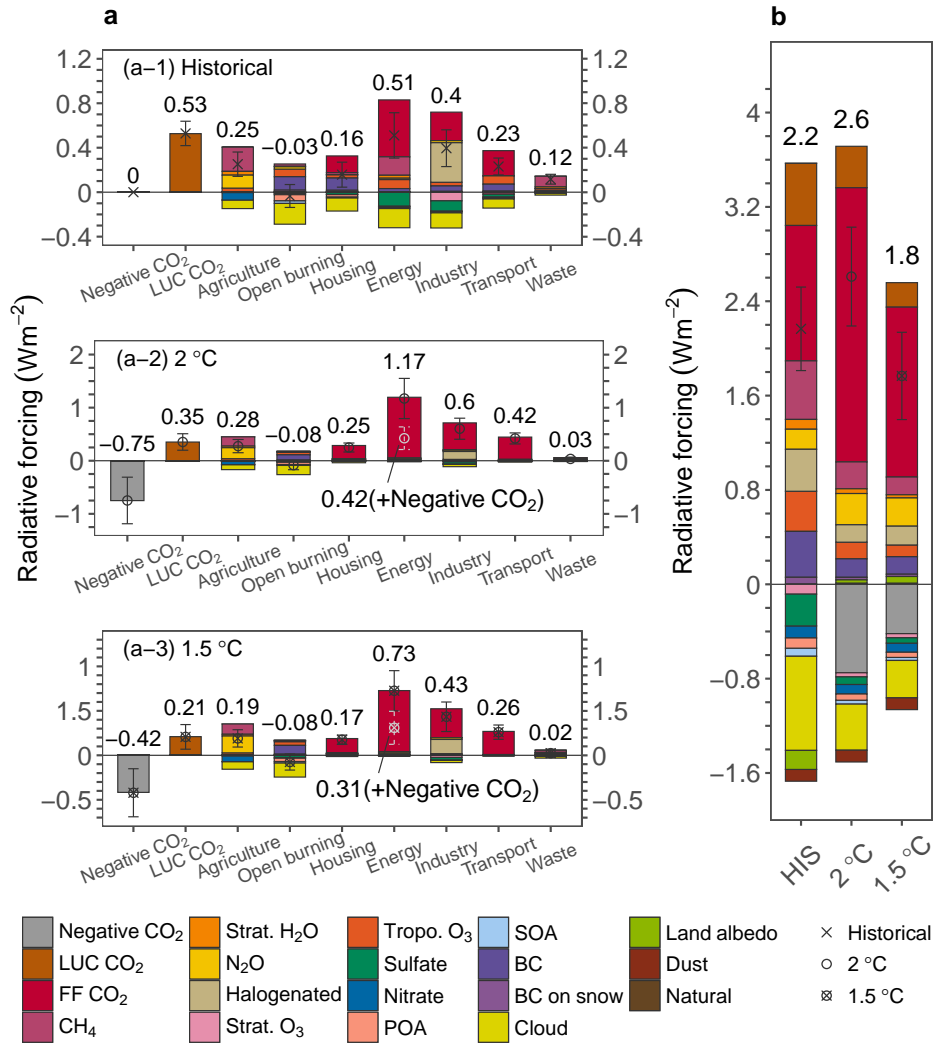


Figure 3. Contributions of the individual climate forcings. a, Sectoral contributions decomposed into individual climate forcings from (a-1) the historical period to 2016, (a-2) the 2 °C climate target by 2100 and (a-3) the 1.5 °C climate target by 2100. Here, open burning sums the agricultural waste burning, forest burning and grass burning levels. Industry includes industry and solvents, similar to in Fig. 2. Transport totals the surface transport, aviation and international shipping values. The annotation values under the energy sector in (a-2) and (a-3) denote the forcing values accounting for the negative CO₂ emissions. b, The world total forcings are decomposed into individual climate forcings. The value on top of the bar indicates the mean value of the total radiative forcing, and the error bar indicates the associated uncertainty resulting from the world ensemble. The direct CO₂ emissions are divided into fossil-fuel CO₂ (FF CO₂), land-use CO₂ (LUC CO₂), and negative CO₂ emissions, if applicable. The natural forcings include solar irradiance and volcanic activity (Fig. S8). The land-use albedo, mineral dust (Dust) and natural forcings are applied to Fig. b only. The probabilities of reaching the 2 °C and 1.5 °C targets here are 56% and 61%, respectively (see Fig. 4). All uncertainties are represented as one standard deviation.

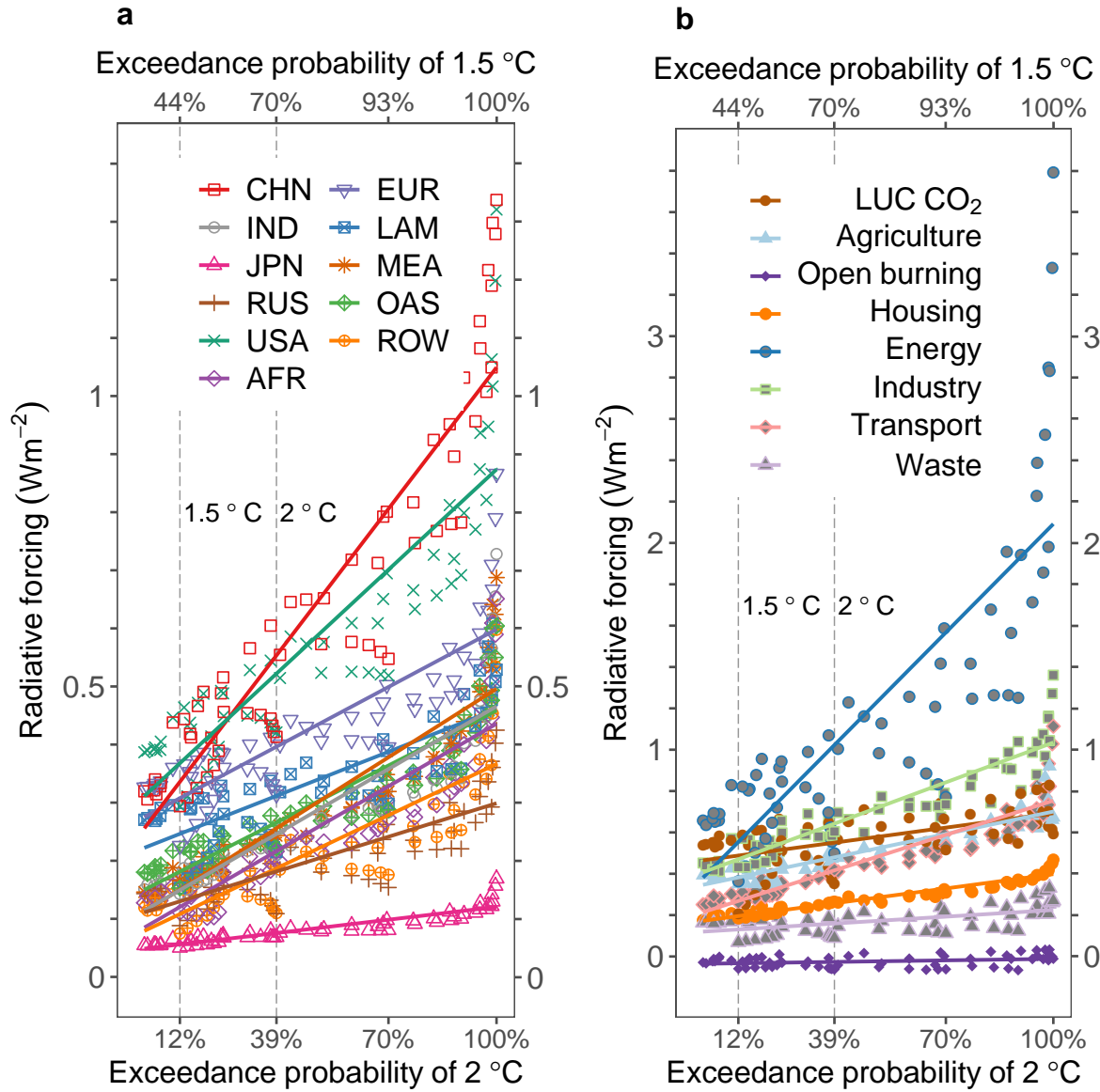


Figure 4. Regional and sectoral contributions under the different future projections. a, The relationship between the exceedance probability of 2°C or 1.5°C and the regional forcing contributions. The color points are the regional relative contributions. The trends are shown by the colored lines obtained via linear regression. b, The relationship between the exceedance probability of 2°C or 1.5°C and the sectoral forcing contributions. The negative CO_2 level is summed into the energy sector to simplify the analysis. The color points are the sectoral forcings. The trends are shown by colored lines obtained through linear regression. The points in Fig. a&b are sampled (from 2020 to 2100, every 10 years) at seven forcing levels, namely, 1.9 Wm^{-2} , 2.6 Wm^{-2} , 3.4 Wm^{-2} , 4.5 Wm^{-2} , 6.0 Wm^{-2} , 7.0 Wm^{-2} and 8.5 Wm^{-2} . The forcing levels are translated into exceedance probabilities within each sample year. The 1.5°C and 2°C results marked with the vertical lines represent the scenarios with forcing levels of 1.9 Wm^{-2} and 2.6 Wm^{-2} , respectively, in 2100.

Acknowledgments

This work was supported by the Integrated Research Program for Advancing Climate Models (TOUGOU), Grant Number JPMXD0717935457, from the Ministry of Education, Culture, Sports, Science and Technology (MEXT), Japan. The computing resources were provided by the Japan Agency for Marine-Earth Science and Technology (JAMSTEC). We thank M. Abe for providing the data used for model calibration and T. Gasser for sharing the OSCAR v2.2 source code.

Author contributions

X.S., K. Tachiiri and K. Tanaka designed the study. X.S. processed the emissions and land cover source data. X.S. developed the model with the help of K. Tanaka and M.W. X.S. performed the calculations and generated the figures. All coauthors contributed to analyzing the results and writing the paper.

Competing financial interests

The authors declare that they have no competing financial interests.

Data availability

The data used to support the analysis are available from the corresponding author upon reasonable request.

- [1] Rogelj J, Popp A, Calvin K V, Luderer G, Emmerling J, Gernaat D, Fujimori S, Strefler J, Hasegawa T, Marangoni G, Krey V, Kriegler E, Riahi K, Van Vuuren D P, Doelman J, Drouet L, Edmonds J, Fricko O, Harmsen M, Havlík P, Humpenöder F, Stehfest E and Tavoni M 2018 *Nature Climate Change* **8** 325–332
- [2] Tanaka K and O'Neill B C 2018 *Nature Climate Change* **8** 319–324
- [3] Rogelj J, Shindell D, Jiang K, Fifita S, Forster P, Ginzburg V, Handa C, Kheshgi H, Kobayashi S, Kriegler E, Mundaca L, SāīfĀīrian R and VilariĀšo M 2018 *Mitigation Pathways Compatible with 1.5 ° C in the Context of Sustainable Development* book section 2, pp 93–174 ISBN ISBN
- [4] Tong D, Zhang Q, Zheng Y, Caldeira K, Shearer C, Hong C, Qin Y and Davis S J 2019 *Nature* **3**
- [5] Tachiiri K, Herran D S, Su X and Kawamiya M 2019 *Environmental Research Letters* **14** 124063
- [6] Kawamiya M, Hajima T, Tachiiri K and Yokohata T 2019 *Progress in Earth and Planetary Science* **0** 0
- [7] Meinshausen M, Meinshausen N, Hare W, Raper S C B, Frieler K, Knutti R, Frame D J and Allen M R 2009 *Nature* **458** 1158–1162
- [8] Myhre G, Shindell D, Breon F M, Collins W, Fuglestedt J, Huang J, Koch D, Lamarque J F, Lee D, Mendoza B, Nakajima T, Robock A, Stephens G, Takemura T and Zhang H 2013 *Anthropogenic and Natural Radiative Forcing* (Cambridge, United Kingdom and New York, NY, USA: Cambridge University Press) book section 8, pp 659–740 ISBN ISBN 978-1-107-66182-0
- [9] Van Vuuren D P, Stehfest E, Gernaat D E, Van Den Berg M, Bijl D L, De Boer H S, Daioglou V, Doelman J C, Edelenbosch O Y, Harmsen M, Hof A F and Van Sluisveld M A 2018 *Nature Climate Change* **8** 391–397
- [10] Seneviratne S I, Rogelj J, Séférian R, Wartenburger R, Allen M R, Cain M, Millar R J, Ebi K L, Ellis N, Hoegh-Guldberg O, Payne A J, Schleussner C F, Tschakert P and Warren R F 2018 *Nature* **558** 41–49
- [11] Rive N and Fuglestedt J S 2008 *Global Environmental Change* **18** 142–152
- [12] den Elzen M G J, Olivier J G J, Höhne N and Janssens-Maenhout G 2013 *Climatic Change* **121** 397–412
- [13] Matthews H D, Graham T L, Keverian S, Lamontagne C, Seto D and Smith T J 2014 *Environmental Research Letters* **9** 1–9
- [14] UNFCCC 2002 Methodological Issues: Scientific and Methodological Assessment of Contributions to Climate Change, Report of the Expert Meeting, Note by the Secretariat Tech. rep. URL <https://unfccc.int/resource/docs/2002/sbsta/inf14.pdf>
- [15] Trudinger C and Enting I 2005 *Climatic Change* **68** 67–99 ISSN 1573-1480
- [16] Skeie R B, Fuglestedt J, Berntsen T, Peters G P, Andrew R, Allen M and Kallbekken S 2017 *Environmental Research Letters* **12** ISSN 17489326
- [17] Fujimori S, Hasegawa T, Ito A, Takahashi K and Masui T 2018 *Scientific Data* **5** 1–13
- [18] Gidden M J, Riahi K, Smith S J, Fujimori S, Luderer G, Kriegler E, Van Vuuren D P, Van Den Berg M, Feng L, Klein D, Calvin K, Doelman J C, Frank S, Fricko O, Harmsen M, Hasegawa T, Havlik P, Hilaire J, Hoesly R, Horing J, Popp A, Stehfest E and Takahashi K 2019 *Geoscientific Model Development* **12** 1443–1475
- [19] Su X, Takahashi K, Fujimori S, Hasegawa T, Tanaka K, Kato E, Shiogama H, Masui T and Emori S 2017 *Earth's Future* **5** 592–604
- [20] Su X, Shiogama H, Tanaka K, Fujimori S, Hasegawa T, Hijioka Y, Takahashi K and Liu J 2018 *Sustainability Science* **13** 291–299
- [21] Höhne N, Blum H, Fuglestedt J, Skeie R B, Kurosawa A, Hu G, Lowe J, Gohar L, Matthews B, de Salles A C N and Ellermann C 2011 *Climatic Change* **106** 359–391
- [22] Li B, Gasser T, Ciais P, Piao S, Tao S, Balkanski Y, Hauglustaine D, Boisier J P, Chen Z, Huang M, Li L Z, Li Y, Liu H, Liu J, Peng S, Shen Z, Sun Z, Wang R, Wang T, Yin G, Yin Y, Zeng H, Zeng Z and Zhou F 2016 *Nature* **531** 357–361
- [23] Lamarque J F, Smith S J, Bond T, Cofala J, Eyring V, Granier C, Heil A, Kainuma M, Klimont Z, Lee D, Lioussé C, Mieville A, Riahi K, Schultz M, Stevenson D, Aardenne J V and van Vuuren D 2009 Historical emissions data (1850 - 2000)
- [24] Gütschow J, Jeffery M L, Gieseke R, Gebel R, Stevens D, Krapp M and Rocha M 2016 *Earth System Science Data* **8** 571–603
- [25] Aardenne J A V, Monni S, Doering U, Olivier J G J and Pagliari V 2018 *Earth System Science Data* **10**

1987–2013

- [26] Hoesly R M, Smith S J, Feng L, Klimont Z, Janssens-Maenhout G, Pitkanen T, Seibert J J, Vu L, Andres R J, Bolt R M, Bond T C, Dawidowski L, Kholod N, Kurokawa J I, Li M, Liu L, Lu Z, Moura M C P, O'Rourke P R and Zhang Q 2018 *Geoscientific Model Development* **11** 369–408
- [27] Hartin C A, Patel P, Schwarber A, Link R P and Bond-Lamberty B P 2015 *Geoscientific Model Development* **8** 939–955
- [28] Kriegler E 2005 *Imprecise probability analysis for integrated assessment of climate change* doctoralthesis Universität Potsdam
- [29] Tanaka K and Kriegler E 2007 Aggregated Carbon cycle, atmospheric chemistry and climate model (ACC2): description of forward and inverse mode Tech. rep. Max Planck Institute for Meteorology
- [30] Wong T E, Bakker A M R, Ruckert K, Applegate P, Slangen A B A and Keller K 2017 *Geoscientific Model Development* **10** 2741–2760
- [31] IPCC 2013 *Annex II: Climate System Scenario Tables* (Cambridge, United Kingdom and New York, NY, USA: Cambridge University Press) book section AII, p 1395–1446
- [32] Gasser T, Ciais P, Boucher O, Quilcaille Y, Tortora M, Bopp L and Hauglustaine D 2017 *Geoscientific Model Development* **10** 271–319
- [33] Sand M, Berntsen T K, Von Salzen K, Flanner M G, Langner J and Victor D G 2016 *Nature Climate Change* **6** 286–289
- [34] Tanaka K, Cavalett O, Collins W J and Cherubini F 2019 *Nature Climate Change* **9** 389–396
- [35] Myhre G and Myhre A 2003 *Journal of Climate* **16** 1511–1524
- [36] Bright R M and Kvalevåg M M 2013 *Atmospheric Chemistry and Physics* **13** 11169–11174
- [37] O'Neill B C, Kriegler E, Ebi K L, Kemp-Benedict E, Riahi K, Rothman D S, van Ruijven B J, van Vuuren D P, Birkmann J, Kok K, Levy M and Solecki W 2017 *Global Environmental Change* **42** 169 – 180
- [38] Kriegler E, Bauer N, Popp A, Humpenöder F, Leimbach M, Strefler J, Baumstark L, Bodirsky B L, Hilaire J, Klein D, Mouratiadou I, Weindl I, Bertram C, Dietrich J P, Luderer G, Pehl M, Pietzcker R, Piontek F, Lotze-Campen H, Biewald A, Bonsch M, Giannousakis A, Kreidenweis U, Müller C, Rolinski S, Schultes A, Schwanitz J, Stevanovic M, Calvin K, Emmerling J, Fujimori S and Edenhofer O 2017 *Global Environmental Change* **42** 297–315
- [39] Ho E, Budescu D V, Bosetti V, van Vuuren D P and Keller K 2019 *Climatic Change* **155** 545–561

Supplemental Materials: Source attributions of radiative forcing by regions, sectors, and climate forcers

Xuanming Su^{1*}, Kaoru Tachiiri^{1,2}, Katsumasa Tanaka^{2,3}, Michio Watanabe¹ & Michio Kawamiya¹

¹Research Institute for Global Change / Research Center for Environmental Modeling and Application / Earth System Model Development and Application Group, Japan Agency for Marine-Earth Science and Technology (JAMSTEC), Yokohama, Japan ²Center for Global Environmental Research, National Institute for Environmental Studies (NIES), Tsukuba, Japan ³Laboratoire des Sciences du Climat et de l'Environnement (LSCE), Commissariat à l'Énergie atomique et aux Énergies alternatives (CEA), Gif-sur-Yvette, France

*To whom correspondence should be addressed; e-mail: suxuanming@jamstec.go.jp.

Supplementary materials

- Model equations for SCM4OPT v2.0
- Table S1 to Table S8
- Fig. S1 to Fig. S15

Model equations for SCM4OPT v2.0

Carbon cycle

The perturbation of the atmospheric carbon pool includes the following five components, as defined in Eq. (1).

- ① CO₂ emissions from fossil fuels and industrial sources;
- ② Anthropogenic CO₂ emissions into or removal from the terrestrial biosphere;
- ③ CH₄ oxidation of fossil fuels;
- ④ Carbon fluxes to or from the terrestrial biosphere due to CO₂ fertilization and climate feedback;
- ⑤ Carbon uptake by oceans.

$$\Delta C_{atm}(t) = E_{CO_2}^{ind}(t) + E_{CO_2}^{lnd}(t) + E_{fCH_4}(t) - F_{bio}(t) - F_{ocn}(t) \quad (1)$$

Terrestrial carbon cycle Both the logarithmic and rectangular hyperbolic forms are adopted to simulate the CO₂ fertilization effects. First, the logarithmic description is defined as:

$$\beta_{log}(t) = 1 + \beta \ln \left(\frac{C_{CO_2}(t)}{C_{CO_2}^0} \right) \quad (2)$$

Second, the rectangular hyperbolic description is given by Eq. (3-5):

$$\beta_{sig-r} = \frac{1 + \beta \log(680/C_{CO_2}^0)}{1 + \beta \log(340/C_{CO_2}^0)} \quad (3)$$

$$\beta_{sig-b} = \frac{(680 - C_b) - \beta_{sig-r}(340 - C_b)}{(\beta_{sig-r} - 1)(680 - C_b)(340 - C_b)} \quad (4)$$

$$\beta_{sig}(t) = \frac{1/(C_{CO_2}^0 - C_b) + \beta_{sig-b}}{1/(C_{CO_2}(t) - C_b) + \beta_{sig-b}} \quad (5)$$

The CO₂ fertilization coefficient (β_{fert}) is given by:

$$\beta_{fert}(t) = (2 - \beta_m)\beta_{log}(t) + (\beta_m - 1)\beta_{sig}(t) \quad (6)$$

The NPP ($F_{NPP}(t)$) and heterotrophic respiration ($F_{rsp}(t)$) are defined as products of the initial carbon flux and a certain fertilization coefficient, considering an exponential temperature feedback effect (Eq. 7 and 8).

$$F_{NPP}(t) = F_{NPP}^0 \beta_{fert}(t) \exp(\sigma_{NPP} \Delta T(t)) \quad (7)$$

$$F_{rsp}(t) = F_{rsp}^0 \beta_{fert}(t) \exp(\sigma_{rsp} \Delta T(t)) \quad (8)$$

The gross land-use emission levels are defined as the sums of the net land-use emissions and the corresponding regrowth, as shown in Eq. (9-11):

$$D_P^{gross}(t) = E_P^{lnd}(t) + G_P(t) \quad (9)$$

$$D_H^{gross}(t) = E_H^{lnd}(t) + G_H(t) \quad (10)$$

$$D_S^{gross}(t) = E_S^{lnd}(t) + G_S(t) \quad (11)$$

Proportions of the net land-use emission levels are allocated as:

- ① Living plant pool;
- ② Detritus pool;
- ③ Soil pool.

Please refer to Eq. (12-14).

$$E_P^{lnd}(t) = \delta_P E_{CO_2}^{lnd}(t) \quad (12)$$

$$E_H^{lnd}(t) = \delta_H E_{CO_2}^{lnd}(t) \quad (13)$$

$$E_S^{lnd}(t) = \delta_S E_{CO_2}^{lnd}(t) \quad (14)$$

The regrowth here is defined to be linearly related to the relaxation time.

$$G_P(t) = a_P + b_P \tau_P(t) \quad (15)$$

$$G_H(t) = a_H + b_H \tau_H(t) \quad (16)$$

$$G_S(t) = a_S + b_S \tau_S(t) \quad (17)$$

The relaxation times are defined as follows:

$$\tau_P(t) = \frac{P_0 - \psi \int_0^t E_P^{lnd}(t') dt'}{dP_0} \quad (18)$$

$$\tau_H(t) = \frac{H_0 - \psi \int_0^t E_H^{lnd}(t') dt'}{dH_0} \quad (19)$$

$$\tau_S(t) = \frac{S_0 - \psi \int_0^t E_S^{lnd}(t') dt'}{dS_0} \quad (20)$$

Therefore, the annual decay rates for the living plant pool, detritus pool and soil pool are defined as shown in Eq. (21-23):

$$dP(t) = C_P(t) \frac{1}{\tau_P(t)} \quad (21)$$

$$dH(t) = C_H(t) \frac{1}{\tau_H(t)} \exp(\sigma_H \Delta T(t)) \quad (22)$$

$$dS(t) = C_S(t) \frac{1}{\tau_S(t)} \exp(\sigma_S \Delta T(t)) \quad (23)$$

The perturbations of carbon in the living plant pool, detritus pool and soil pool at time t are defined as shown in Eq. (24-26):

$$\Delta P(t) = F_{NPP}(t)\nu_P - dP(t) - D_P^{gross}(t) - F_{rsp}(t) \quad (24)$$

$$\Delta H(t) = F_{NPP}(t)\nu_H - dH(t) - D_H^{gross}(t) + dP(t)\rho_{p2d} \quad (25)$$

$$\Delta S(t) = F_{NPP}(t)\nu_S - dS(t) - D_S^{gross}(t) + dP(t)\rho_{p2s} + dH(t)\delta_{d2s} \quad (26)$$

Therefore, the carbon flux to or from the terrestrial biosphere can be calculated as follows:

$$F_{bio}(t) = \Delta P(t) + \Delta H(t) + \Delta S(t) \quad (27)$$

Here, we fitted the land net primary productivity (NPP), land surface net downward carbon flux (NBP), ocean surface downward carbon flux (fgco2) and CO₂ concentration of SCM4OPT v2.0 to the outputs of three CMIP5 experiments, namely, the historical, RCP26 and RCP85 experiments. The calibration procedures were performed in several steps, thereby minimizing the sum of squared errors (SSEs) with the associated variables.

Oceanic carbon cycle We apply the method proposed by [1, 2] to construct the oceanic carbon cycle (Eq.28-39).

$$\begin{aligned} DIC(obs, t) \cdot \left(\frac{K_1(obs, t)}{H(obs, t)} + 2 \frac{K_1(obs, t)K_2(obs, t)}{H(obs, t)^2} \right) = \\ \left(ALK(obs, t) - \frac{K_B(obs, t)BOR(obs)}{K_B(obs, t) + H(obs, t)} - \frac{K_W(obs, t)}{H(obs, t)} + H(obs, t) \right) \cdot \\ \left(1 + \frac{K_1(obs, t)}{H(obs, t)} + \frac{K_1(obs, t)K_2(obs, t)}{H(obs, t)^2} \right) \end{aligned} \quad (28)$$

$$CO_2^{sys}(obs, t) = \frac{DIC(obs, t)}{1 + \frac{K_1(obs, t)}{H(obs, t)} + \frac{K_1(obs, t)K_2(obs, t)}{H(obs, t)^2}} \quad (29)$$

$$pCO_2(obx, t) = \frac{CO_2^{sys}(obx, t)}{K_H(obx, t)} \quad (30)$$

$$HCO_3(obx, t) = \frac{DIC(obx, t)}{1 + \frac{H(obx, t)}{K_1(obx, t)} + \frac{K_2(obx, t)}{H(obx, t)}} \quad (31)$$

$$CO_3(obx, t) = \frac{DIC(obx, t)}{1 + \frac{H(obx, t)}{K_2(obx, t)} + \frac{H(obx, t)^2}{K_1(obx, t)K_2(obx, t)}} \quad (32)$$

$$K_1(obx, t) = \frac{H(obx, t)HCO_3(obx, t)}{CO_2^{sys}(obx, t)} \quad (33)$$

$$K_2(obx, t) = \frac{H(obx, t)CO_3(obx, t)}{HCO_3(obx, t)} \quad (34)$$

$$K_B(obx, t) = \frac{H(obx, t)BOH_4(obx)}{BOH_3(obx)} \quad (35)$$

$$BOR(obx) = 416.0 \cdot \frac{S}{35.0} = BOH_4(obx) + BOH_3(obx) \quad (36)$$

$$K_W(obx, t) = \frac{H(obx, t)}{OH(obx, t)} \quad (37)$$

$$F_{as}(obx, t) = \kappa_s \alpha_s \cdot (C_{CO_2}(t) - pCO_2(obx, t)) \quad (38)$$

$$F_{ocn}(t) = \sum_{obx} F_{as}(obx, t) \quad (39)$$

The carbon in the atmospheric pool is converted into the CO₂ concentration by:

$$C_{CO_2}(t) = \frac{C_{atm}(t)}{\alpha_{ppm2gtc}} \quad (40)$$

The radiative forcing from CO₂ can be obtained as:

$$f_{CO_2}(t) = \alpha_{CO_2} \log \frac{C_{CO_2}(t)}{C_{CO_2}^0} \quad (41)$$

CH₄

The change in the CH₄ concentration is directly calculated from the CH₄ emissions from natural, industrial and land-use sources and from the CH₄ sinks in the troposphere (based on the lifetime of OH), stratosphere, and soil.

$$\Delta C_{CH_4}(t) = \frac{E_{CH_4}^{nat} + E_{CH_4}^{ind}(t) + E_{CH_4}^{lnd}(t)}{\theta_{CH_4}} - \frac{C_{CH_4}(t-1)}{\tau_{CH_4}^{tot}(t-1)} \quad (42)$$

$$\frac{1}{\tau_{CH_4}^{tot}(t)} = \frac{1}{\tau_{CH_4}^{init}/\tau_{OH}^{rel}(t)} + \frac{1}{\tau_{CH_4}^{soil}} + \frac{1}{\tau_{CH_4}^{oth}} \quad (43)$$

The change in the tropospheric OH abundance relative to the level in 2000 is thus modeled as:

$$\begin{aligned} \tau_{OH}^{rel}(t) = & S_{\tau_{CH_4}} \Delta T_{2k}(t) + \left(\frac{C_{CH_4}(t)}{C_{CH_4}^{2k}} \right)^{S_{CH_4}^{OH}} \\ & \cdot \exp \left(S_{NO_x}^{OH} \Delta E_{NO_x}(t) + S_{CO}^{OH} \Delta E_{CO}(t) + S_{VOC}^{OH} \Delta E_{VOC}(t) \right) \end{aligned} \quad (44)$$

N₂O

The feedback effect of the atmospheric N₂O concentration on its own lifetime is approximated as:

$$\tau_{N_2O}(t) = \tau_{N_2O}^{init} \left(\frac{C_{N_2O}(t)}{C_{N_2O}^{2k}} \right)^{S_{\tau_{N_2O}}} \quad (45)$$

The change in the atmospheric N₂O concentration is calculated as:

$$\Delta C_{N_2O}(t) = \frac{E_{N_2O}^{nat} + E_{N_2O}^{ind}(t) + E_{N_2O}^{lnd}(t)}{\theta_{N_2O}} - \frac{C_{N_2O}(t-1)}{\tau_{N_2O}(t-1)} \quad (46)$$

The radiative forcings of CH₄ ($f_{CH_4}(t)$) and N₂O ($f_{N_2O}(t)$) are calculated following the standard IPCC (2001) methods [3], as shown in Eq. (47-49):

$$\begin{aligned} f_{CH_4}(t) = & \alpha_{CH_4} \left(\sqrt{C_{CH_4}(t)} - \sqrt{C_{CH_4}^0} \right) - \\ & (f_{mn}(C_{CH_4}(t), C_{N_2O}^0) - f_{mn}(C_{CH_4}^0, C_{N_2O}^0)) \end{aligned} \quad (47)$$

$$\begin{aligned} f_{N_2O}(t) = & \alpha_{N_2O} \left(\sqrt{C_{N_2O}(t)} - \sqrt{C_{N_2O}^0} \right) - \\ & (f_{mn}(C_{CH_4}^0, C_{N_2O}(t)) - f_{mn}(C_{CH_4}^0, C_{N_2O}^0)) \end{aligned} \quad (48)$$

The function $f_{mn}(M, N)$ defining the overlap between CH_4 and N_2O is:

$$f_{mn}(M, N) = 0.47 \log \left(1 + 0.6356 \left(\frac{MN}{10^6} \right)^{0.75} + 0.007 \frac{M}{10^3} \left(\frac{MN}{10^6} \right)^{1.52} \right) \quad (49)$$

Halogenated gases

All the available halogenated gases are treated separately with regard to their concentrations [1, 4]:

$$C_{hc}(t+1, hc) = \tau_{hc} \frac{E(t, hc)}{\mu_{hc}} \frac{\rho_{atm}}{m_{atm}} \cdot \left(1 - \exp\left(-\frac{1}{\tau_{hc}}\right) \right) + C_{hc}(t, hc) \left(1 - \exp\left(-\frac{1}{\tau_{hc}}\right) \right) \quad (50)$$

The radiative forcing from each halogenated gas is given by:

$$f_{hc}(t, hc) = \alpha_{hc} (C_{hc}(t, hc) - C_{hc}^0) \quad (51)$$

Direct effect of aerosols

We update the estimation of the direct effects from aerosols based on [5]. The change in the sulfate burden is assessed to capture the radiative forcing impacts resulting from sulfate aerosols.

$$C_{SO_4}(t) = C_{SO_4}^0 + \alpha_{SO_4} \tau_{SO_2} (E_{SO_2}^{ind}(t) + E_{SO_2}^{lnd}(t)) + \alpha_{SO_4} \tau_{dms} E_{dms}(t) + \Gamma_{SO_4} \Delta T_{as}(t) \quad (52)$$

Similarly, the concentration of primary organic aerosols (POAs) is defined as:

$$C_{POA}(t) = C_{POA}^0 + \tau_{OM}^{ind} \alpha_{POM} E_{OC}^{ind}(t) + \tau_{OM}^{lnd} \alpha_{POM} E_{OC}^{lnd}(t) + \Gamma_{POA} \Delta T_{as}(t) \quad (53)$$

The black carbon (BC) concentration is:

$$C_{BC}(t) = C_{BC}^0 + \tau_{BC}^{ind} E_{BC}^{ind}(t) + \tau_{BC}^{lnd} E_{BC}^{lnd}(t) + \Gamma_{BC} \Delta T_{as}(t) \quad (54)$$

The concentration of nitrate aerosols is:

$$C_{NO_3}(t) = C_{NO_3}^0 + \tau_{NO_x} (E_{NO_x}^{ind}(t) + E_{NO_x}^{lnd}(t)) + \tau_{NH_3} (E_{NH_3}^{ind}(t) + E_{NH_3}^{lnd}(t)) + \Gamma_{NO_3} \Delta T_{as}(t) \quad (55)$$

The concentration of secondary organic aerosols (SOAs) is:

$$C_{SOA}(t) = C_{SOA}^0 + \tau_{VOC} (E_{VOC}^{ind}(t) + E_{VOC}^{lnd}(t)) + \tau_{BVOC} E_{BVOC}(t) + \Gamma_{SOA} \Delta T_{as}(t) \quad (56)$$

Thus, the direct radiative forcing caused by aerosols and pollutants is:

$$f_{aero}(t) = \alpha_{aero}^{rf} \delta C_{aero}(t) \quad (57)$$

Mineral dust aerosols

The historical radiative forcing from mineral dust aerosols is obtained from MAGICC 6.0 [4]. The future forcing level is assumed to remain at a constant value of -0.1 Wm^{-2} after 2005.

$$f_{mindust}(t) = -0.1 \quad (58)$$

Cloud effects

The tropospheric burden of soluble aerosols can be obtained by:

$$C_{solu}(t) = C_{solu}^0 + \sum_{aero \in SO_4, POA, BC, NO_3, SOA} \alpha_{solu}^{aero} (C_{aero}(t) - C_{aero}^0) \quad (59)$$

The cloud forcing effects are estimated by:

$$f_{cloud}(t) = f_{BC}(t) \kappa_{adj}^{BC} + \phi_{solu} \ln \left(1 + \frac{\Delta C_{solu}(t)}{C_{solu}^0} \right) \quad (60)$$

Stratospheric ozone

The equivalent effective stratospheric chlorine (EESC) concentration is calculated as:

$$C_{EESC}(t) = a_{EESC} \left(\sum_{Cl} n_{Cl} f_{Cl} C_{hc}(t, Cl) + \alpha_{br} \sum_{Br} n_{Br} f_{Br} C_{hc}(t, Br) \right) \quad (61)$$

The concentration of stratospheric ozone is:

$$C_{O3s}(t) = C_{O3s}^0 + \xi_{EESC}^{O3s} (C_{EESC}(t) - C_{EESC}^0) + \xi_{N2O}^{O3s} \left(1 - \frac{C_{EESC}(t) - C_{EESC}^0}{C_{EESC}^X} \right) \Delta C_{N2O}^{lag}(t) + \Gamma_{O3s} \Delta T_{as}(t) \quad (62)$$

Thus, the forcing effect of the stratospheric ozone burden can be obtained by:

$$f_{O3s}(t) = \alpha_{O3s}^{rf} (C_{O3s}(t) - C_{O3s}^0) \quad (63)$$

Tropospheric ozone

The tropospheric ozone concentration is estimated to be:

$$C_{O3t}(t) = C_{O3t}^0 + \xi_{CH4}^{O3t} \ln \left(1 + \frac{\Delta C_{CH4}(t)}{C_{CH4}^0} \right) + \Gamma_{O3t} \Delta T_{as}(t) + \sum_{aero \in NO_x, CO, VOC} \xi_{aero}^{O3t} (E_{aero}^{ind}(t) + E_{aero}^{lnd}(t)) \quad (64)$$

The radiative forcing from the tropospheric ozone is then calculated as:

$$f_{O3t}(t) = \alpha_{O3t}^{rf} (C_{O3t}(t) - C_{O3t}^0) \quad (65)$$

Stratospheric water vapor from CH₄ oxidation

The forcing effect of the stratospheric water vapor from CH₄ oxidation $f_{H2O}(t)$ is calculated by:

$$f_{H2O}(t) = \alpha_{H2O}^{rf} \sqrt{C_{CH4}^0} \left(\sqrt{1 + \frac{\Delta C_{CH4}^{lag}(t)}{C_{CH4}^0}} - 1 \right) \quad (66)$$

Land-use albedo

The forcing effect from the land-use albedo is estimated according to the annual mean albedo at the biome and regional scales, using the changes in regional land cover as input following the methods described in ref [5].

$$f_{LCC}(t) = -\pi_{trans} \phi_{rds} \sum_{bio} \alpha_{LCC}^{bio} \frac{\Delta A_{LCC}^{bio}(t)}{\Delta A_{Earth}} \quad (67)$$

BC on snow

The forcing effect of BC on snow is determined as a linear function of the BC emission level:

$$f_{BCSnow}(t) = a_{BC} + b_{BC} (E_{BC}^{ind}(t) + E_{BC}^{lnd}(t)) \quad (68)$$

Natural sources

Regarding the various natural sources, the volcanic and solar forcings are assumed to be the natural forcing inputs for CMIP6.

$$f_{volc}(t) = f_{volc}^{CMIP6}(t) \quad (69)$$

$$f_{solar}(t) = f_{solar}^{CMIP6}(t) \quad (70)$$

Global mean temperature

The estimation of the global mean temperature is based on the Diffusion Ocean Energy balance CLIMate (DOECLIM) model by using the total radiative forcing as input [6, 7]. Here, we reestimated the climate sensitivity, vertical ocean diffusivity and radiative forcing coefficient for CO₂ doubling based on the CMIP5 outputs related to each available GCM. The detailed descriptions and equations are contained in the references [6, 7].

For the simple climate module, the time step was calibrated to be 1/6 year for SCM4OPT v2.0 to avoid possible convergence problems when calculating the ocean carbon cycle [1]. The calibrated results are shown in Figs. S5 to S11. We also included the results produced by other models or associated statistical records for comparison purposes.

Nomenclature

Aerosol and pollutants

α_{aero}^{rf} Radiative efficiency for aerosol *aero*

α_{POM} Conversion of POM from Tg(OC) to Tg(OM)

α_{SO_4} Conversion of SO_4 from TgS to Tg(SO₄)

α_{solu}^{aero} Soluble fraction for aerosol *aero*

$\delta C_{aero}(t)$ Aerosol *aero* concentration in time *t*

$\Delta T_{as}(t)$ Global mean temperature relative to 1850 in time *t*

Γ_{BC} BC sensitivity to global mean temperature

Γ_{NO_3} NO_x sensitivity to global mean temperature

Γ_{POA} Primary organic aerosol sensitivity to global mean temperature

Γ_{SO_4} Sulfate sensitivity to global mean temperature

Γ_{SOA}	NMVOCs sensitivity to global mean temperature
κ_{adj}^{BC}	Adjustment coefficient of BC radiative forcing to cloud forcing effect
ϕ_{solu}	Intensity effect coefficient for soluble aerosols
τ_{BC}^{ind}	Lifetime of industrial BC
τ_{BC}^{lnd}	Lifetime of land use BC
τ_{BVOC}	Lifetime of biogenic NMVOCs
τ_{dms}	Lifetime of dimethyl sulfide
τ_{NH_3}	Lifetime of NH_3
τ_{NO_x}	Lifetime of NO_x
τ_{OM}^{ind}	Lifetime of industrial primary organic aerosols
τ_{OM}^{lnd}	Lifetime of land use primary organic aerosols
τ_{SO_2}	Lifetime of SO_2
τ_{VOC}	Lifetime of NMVOCs
$C_{aero}(t)$	Aerosol concentration in time t
C_{aero}^0	Initial aerosol concentration
$C_{BC}(t)$	Concentration of BC in time t
C_{BC}^0	Initial concentration of BC
$C_{NO_3}(t)$	Concentration of nitrate aerosols in time t
$C_{NO_3}^0$	Initial concentration of nitrate aerosols
$C_{POA}(t)$	Concentration of primary organic aerosols in time t
C_{POA}^0	Initial concentration of primary organic aerosols
$C_{SO_4}(t)$	Sulfate concentration in time t
$C_{SO_4}^0$	Initial sulfate concentration
$C_{SOA}(t)$	Concentration of SOA in time t
C_{SOA}^0	Initial concentration of SOA
$C_{solu}(t)$	Number concentrations for soluble aerosol in time t
C_{solu}^0	Initial number concentrations for soluble aerosol
$E_{BC}^{ind}(t)$	Industrial BC emissions in time t
$E_{BC}^{lnd}(t)$	Land use BC emissions in time t
$E_{BVOC}(t)$	Biogenic NMVOC emissions in time t
$E_{dms}(t)$	Dimethyl sulfide emissions
$E_{NH_3}^{ind}(t)$	Industrial NH_3 emissions in time t
$E_{NH_3}^{lnd}(t)$	Land use NH_3 emissions in time t
$E_{NO_x}^{ind}(t)$	Industrial NO_x emissions in time t
$E_{NO_x}^{lnd}(t)$	Land use NO_x emissions in time t
$E_{OC}^{ind}(t)$	Industrial OC emissions in time t

$E_{OC}^{lnd}(t)$ Land use OC emissions in time t

$E_{SO_2}^{ind}(t)$ Industrial SO_2 emissions in time t

$E_{SO_2}^{lnd}(t)$ Land use SO_2 emissions in time t

$E_{VOC}^{ind}(t)$ Industrial NMVOC emissions in time t

$E_{VOC}^{lnd}(t)$ land use NMVOC emissions in time t

$f_{aero}(t)$ Direct radiative forcing for aerosol $aero$ in time t

$f_{BC}(t)$ BC radiative forcing in time t

$f_{cloud}(t)$ Cloud forcing effects in time t

$f_{mindust}(t)$ Radiative forcing from mineral dust

CO₂

α_{CO_2} Forcing scaling parameter, $= \frac{3.71}{\log(2)} = 5.35 \text{ Wm}^{-2}$ [8]

$\alpha_{ppm2gtc}$ Unit conversion factor from ppm to GtC, $= 2.123 \text{ GtC ppm}^{-1}$

α_s Solubility of CO₂ in seawater

β CO₂ fertilization factor

β_{fert} CO₂ fertilization coefficient

β_{log} Fertilization coefficient

β_m Allocation coefficient between the two descriptions of the CO₂ fertilization effects

$\beta_{sig}(t)$ Effective CO₂ fertilization factor at time t

$\Delta C_{atm}(t)$ Atmospheric carbon pool in time t

$\Delta P(t)$, $\Delta H(t)$ and $\Delta S(t)$ Total changes in the carbon levels for the living plant pool, the detritus pool and the soil pool

δ_{d2s} Fraction of $dH(t)$ that goes to the soil pool

δ_i land-use emission distribution factors

κ_s CO₂ transfer velocity

ν_P , ν_H and $\nu_S=1-\nu_P-\nu_H$ NPP partition factors for the living plant pool, the detritus pool and the soil pool

ψ Fraction of gross deforestation without regrowth

ρ_{p2d} and $\rho_{p2s}=1-\rho_{p2d}$ Fractions of $dP(t)$ that are distributed to the detritus and soil pools, respectively

σ_H and σ_S Temperature feedback coefficients for detritus pool and soil pool

σ_{rsp} Sensitivity to changes in temperature

$\tau_i(t)$ Regrowth relaxation time, a_i and b_i are parameters that are estimated based the CMIP5 outputs

$ALK(obx, t)$ Total alkalinity for ocean box obx and time t

$BOH_3(obx)$ Ocean boric acid

$BOH_4(obx)$ Ocean borate

$BOR(obx)$ Total boron for ocean box obx
 C_b Concentration at which the NPP is zero, which is taken to be 31 ppm [9]
 $C_{CO_2}(t)$ Atmospheric CO_2 concentration in time t
 $C_{CO_2}(t)$ CO_2 concentration
 $C_{CO_2}^0$ Pre-industrial CO_2 concentration (278 ppm)
 $C_P(t)$, $C_H(t)$ and $C_S(t)$ Amounts of carbon remaining in the living plant pool, detritus pool and soil pool
 $CO_2^{sys}(obx, t)$ Dissolved inorganic (DIC) of the system for ocean box obx and time t
 $CO_3(obx, t)$ Concentration of ocean carbonate CO_3^{2-} for ocean box obx and time t
 $D_i^{gross}(t)$ Gross land-use emission level, $i \in \{P, H, S\}$ denote the living plant pool, the detritus pool and the soil pool, respectively
 $DIC(obx, t)$ Dissolved inorganic for ocean box obx and time t
 dP_0 , dH_0 and dS_0 Initial decay rates
 $E_{CO_2}^{ind}(t)$ CO_2 emissions from fossil fuels and industrial sources
 $E_{CO_2}^{lnd}(t)$ Anthropogenic CO_2 from or removal to the terrestrial biosphere
 $E_H^{lnd}(t)$ Detritus pool
 $E_i^{lnd}(t)$ Net land-use emission level, $i \in \{P, H, S\}$ denote the living plant pool, the detritus pool and the soil pool, respectively
 $E_P^{lnd}(t)$ Living plant pool
 $E_S^{lnd}(t)$ Soil pool
 $E_{fCH_4}(t)$ CH_4 oxidation of fossil fuels
 F_{rsp}^0 Pre-industrial heterotrophic respiration
 $F_{as}(obx, t)$ Carbon fluxes between the atmosphere and surface ocean box for ocean box obx and time t , if applicable
 $F_{bio}(t)$ Carbon flux to or from the terrestrial biosphere
 $F_{bio}(t)$ Carbon fluxes to or from the terrestrial biosphere due to CO_2 fertilization and climate feedback
 $f_{CO_2}(t)$ CO_2 radiative forcing in time t
 $F_{NPP}(t)$ Net primary productivity (NPP) in time t
 $F_{ocn}(t)$ Carbon uptake by the ocean in time t
 $F_{rsp}(t)$ Heterotrophic respiration in time t
 $G_i(t)$ Carbon flux originating from regrowth, $i \in \{P, H, S\}$ denote the living plant pool, the detritus pool and the soil pool, respectively
 $G_i(t)$ Land use regrowth, a_i and b_i are parameters that are estimated based the CMIP5 outputs
 $H(obx, t)$ Concentration of $[H^+]$ for ocean box obx and time t
 $HCO_3(obx, t)$ Concentration of ocean bicarbonate HCO_3^- for ocean box obx and time t

$K_1(obx, t)$ First acidity constant of carbonic acid for ocean box obx and time t

$K_2(obx, t)$ Second acidity constant of carbonic acid for ocean box obx and time t

$K_B(obx, t)$ Dissociation constant of boric acid for ocean box obx and time t

$K_H(obx, t)$ Henry's constant for ocean box obx and time t

$K_W(obx, t)$ Dissociation constant of water for ocean box obx and time t

$OH(obx, t)$ Concentration of OH^{-1}

P_0, H_0 and S_0 Initial states of the living plant pool, the detritus pool and the soil pool

$pCO_2(obx, t)$ Sea surface partial pressure for ocean box obx and time t

Other GHG emissions

α_{CH_4} CH_4 scaling factors, =0.036

α_{hc} Halogenated gas radiative efficiency

α_{N_2O} N_2O scaling factors, =0.12

$\Delta C_{CH_4}(t)$ Change in the CH_4 concentration in time t

$\Delta C_{N_2O}(t)$ N_2O concentration change in time t

$\Delta T_{2k}(t)$ Temperature change above the 2000 level

μ_{hc} Molar mass of halogenated gas hc

ρ_{atm} Average density of air

$\tau_{CH_4}^{init}$ Initial lifetime of OH , =9.6 years

$\tau_{CH_4}^{init} / \tau_{OH}^{rel}(t)$ CH_4 lifetimes in the troposphere

$\tau_{N_2O}^{init}$ Initial N_2O lifetime, =120 years

$\tau_{CH_4}^{oth}$ CH_4 lifetimes in stratosphere, =120 years

$\tau_{CH_4}^{soil}$ CH_4 lifetimes in soil, =160 years

$\tau_{CH_4}^{tot}(t)$ CH_4 lifetime in time t

τ_{hc} Lifetime of halogenated gas hc

$\tau_{N_2O}(t)$ N_2O lifetime in time t

θ_{CH_4} CH_4 conversion factor, 2.78 Tg ppb⁻¹

θ_{N_2O} N_2O conversion factor, =4.81 Tg ppb⁻¹

$C_{CH_4}^0$ CH_4 pre-industrial concentration, =721.9 ppb

C_{hc}^0 Halogenated gas pre-industrial atmospheric concentration

$C_{N_2O}^0$ N_2O pre-industrial concentration, =273.0 ppb

$C_{CH_4}^{2k}$ CH_4 concentration in the year 2000

$C_{N_2O}^{2k}$ N_2O concentration in the year 2000

$C_{hc}(t + 1, hc)$ Concentration (in ppt) of halogenated gas hc in year $t + 1$

$C_{N_2O}(t)$ N_2O concentration

$E(t, hc)$ Halogenated gas emission level of hc in kt yr⁻¹

$E_{CH_4}^{ind}(t)$ Industrial CH_4 emissions in time t

$E_{N_2O}^{ind}(t)$ Industrial N_2O emissions in time t
 $E_{CH_4}^{ind}(t)$ Land-use sources CH_4 emissions in time t
 $E_{N_2O}^{ind}(t)$ Land-use sources N_2O emissions in time t
 $E_{CH_4}^{nat}$ Natural CH_4 emissions, =274.5 Mt CH_4 yr⁻¹
 $E_{N_2O}^{nat}$ Natural N_2O emissions, =8.4 Mt N_2O -N yr⁻¹
 $f_{hc}(t, hc)$ Halogenated gas radiative forcing
 M and N CH_4 and N_2O concentration inputs
 m_{atm} Total mass of the atmosphere
 S_x^{OH} Sensitivities of the tropospheric OH to CH_4 , NO_x , CO and VOC, with values of -0.32, +0.0042, -1.05E-4 and -3.15E-4, respectively
 $S_{\tau_{CH_4}}$ CH_4 temperature sensitivity coefficient of tropospheric chemical reactions, =0.0316 °C⁻¹ [4]
 $S_{\tau_{N_2O}}$ N_2O sensitivity coefficient, =-0.05

Ozone

α_{br} Ratio of effectiveness in ozone depletion between bromine and chlorine
 α_{O3s} Stratospheric ozone radiative efficiency
 α_{O3t} Tropospheric ozone radiative efficiency
 $\Delta C_{N_2O}^{lag}(t)$ N_2O concentration with time-lag in time t
 Γ_{O3s} Stratospheric ozone sensitivity to global mean temperature
 Γ_{O3t} Tropospheric ozone sensitivity to global mean temperature
 ξ_{aero}^{O3t} Tropospheric ozone sensitivity of aerosol *aero*
 $\xi_{CH_4}^{O3t}$ Tropospheric ozone sensitivity of CH_4 effect
 ξ_{EESC}^{O3s} Stratospheric ozone sensitivity to EESC
 $\xi_{N_2O}^{O3s}$ Stratospheric ozone sensitivity to N_2O
 a_{EESC} A fractional release factor of the EESC
 $C_{EESC}(t)$ EESC concentration in time t
 C_{EESC}^0 Initial EESC concentration
 C_{EESC}^X Non-linear interaction parameter between chlorine and nitrogen chemistries
 $C_{hc}(t, Cl)$ and $C_{hc}(t, Br)$ Gas mixing rates in the stratosphere for chlorine and bromine
 $C_{O3s}(t)$ Stratospheric ozone concentration in time t
 C_{O3s}^0 Initial stratospheric ozone concentration
 $C_{O3t}(t)$ Tropospheric ozone concentration in time t
 C_{O3t}^0 Initial tropospheric ozone concentration
 f_{Cl} and f_{Br} Release efficiencies of stratospheric halogens for chlorine and bromine
 $f_{O3s}(t)$ Forcing effect of stratospheric ozone burden in time t
 $f_{O3t}(t)$ Radiative forcing of tropospheric ozone in time t

n_{Cl} and n_{Br} Numbers of chlorine and bromine atoms, respectively

Surface albedo

α_{LCC}^{bio} Yearly averaged albedo at the for biome

ΔA_{Earth} Surface area of the Earth

$\Delta A_{LCC}^{bio}(t)$ Surface area change for biome in time t

ϕ_{rds} Radiative short-wave and downward flux at the surface

π_{trans} Global short-wave and upward transmittance

$f_{LCC}(t)$ Land-use albedo forcing in time t

Other

$\alpha_{H_2O}^{rf}$ Stratospheric water vapor radiative efficiency

$\Delta C_{CH_4}^{lag}(t)$ CH_4 concentration with time lag in time t

a_{BC} and b_{BC} Forcing scaling parameters of the BC on snow

$f_{BCSnow}(t)$ Forcing effect of the BC on snow

$f_{H_2O}(t)$ Forcing effect of the stratospheric water vapor from CH_4 oxidation in time t

$f_{solar}(t)$ Solar irradiance forcing effects in time t

$f_{solar}^{CMIP6}(t)$ Solar irradiance forcing effects for CMIP6 in time t

$f_{volc}(t)$ Volcanic forcing effects in time t

$f_{volc}^{CMIP6}(t)$ Volcanic forcing effects for CMIP6 in time t

Table S1. Datasets of historical emissions

Source	Period	Emission	Format	Reference
CEDS	1750-2014	CO ₂ , CH ₄ , BC, CO, NH ₃ , NMVOC, NO _x , OC, SO ₂	Spatial (sectoral)	Ref [10]
EDGAR v4.3.2	1970-2012	CO ₂ , CH ₄ , N ₂ O, BC, CO, NH ₃ , NMVOC, NO _x , OC, SO ₂	Regional and sectoral /Spatial (sectoral)	Ref [11]
EDGAR v4.2 (*)	1970-2008	CO ₂ , CH ₄ , N ₂ O, CO, NH ₃ , F-gases, NF ₃ , SF ₆ , NMVOC, NO _x , SO ₂	Regional and sectoral /Spatial (sectoral)	Ref [12]
PRIMAP v2.0 (**)	1850-2016	CO ₂ , CH ₄ , N ₂ O, F-gases, HFCs, PFCs, NF ₃ , SF ₆	Spatial (sectoral)	Ref [13]
RCP historical	1850-2000	CH ₄ , BC, CO, NH ₃ , NO _x , OC, SO ₂ , VOC	Spatial (sectoral)	Ref [14]

(*) Halogenated gas emissions are used in EDGAR v4.3.2 since these emissions are not included in EDGAR v4.3.2.

(**) N₂O is employed in the other datasets when not included.

Table S2. Datasets of the future scenarios at the various forcing levels

Forcing levels (Wm ⁻²)	Source	Scenario	Reference
1.9	AIM/CGE	SSP1-1.9, SSP2-1.9	Ref [15]
1.9	IAMC	SSP1-1.9	Ref [16]
2.6	AIM/CGE	SSP1-2.6, SSP2-2.6, SSP3-2.6(*), SSP4-2.6, SSP5-2.6	Ref [15]
2.6	IAMC	SSP1-2.6, Ref [16]	
3.4	AIM/CGE	SSP1-3.4, SSP2-3.4, SSP3-3.4, SSP4-3.4, SSP5-3.4	Ref [15]
3.4	IAMC	SSP4-3.4, SSP5-3.4-OS	Ref [16]
4.5	AIM/CGE	SSP1-4.5, SSP2-4.5, SSP3-4.5, SSP4-4.5, SSP5-4.5	Ref [15]
4.5	IAMC	SSP2-4.5	Ref [16]
6.0	AIM/CGE	SSP1-Baseline, SSP2-6.0, SSP3-6.0, SSP4-Baseline, SSP5-6.0	Ref [15]
6.0	IAMC	SSP3-LowNTCF(**), SSP4-6.0	Ref [16]
7.0	AIM/CGE	SSP2-Baseline, SSP3-Baseline	Ref [15]
7.0	IAMC	SSP3-7.0	Ref [16]
8.5	AIM/CGE	SSP5-Baseline	Ref [15]
8.5	IAMC	SSP5-8.5	Ref [16]

(*) The SSP3-2.6 scenario was not available in Table 2 in ref [15], however, the dataset was provided in <https://doi.org/10.7910/DVN/4NVGWA>. We retained SSP3-2.6 in our analysis.

(**) The target forcing level of SSP3-LowNTCF was 6.3 Wm⁻² (Table 1 in ref [16]). We classified it to the closest forcing level of 6.0 Wm⁻².

Table S3. Datasets of CO₂ emissions from land-use change

Source	Period	Format	Reference
Houghton et al. (2012) (*)	1960-2010	Regional	Ref [17, 18]
MPIMET	1850-2005	Spatial grid	Ref [19]
PRIMAP v1.2	1850-2015	Regional	Ref [13]
Smith and Rothwell (2013)	1850-2010	Regional	Ref [20]

(*) An updated version [18] was used, downloaded from <http://www.globalcarbonatlas.org/en/CO2-emissions>.

Table S4. Please refer to the spreadsheet in the supplementary tables. Atmospheric drivers and radiative forcings. Note: This table is compiled based on Figure SPM.5 in IPCC (2013) and references Gasser et al. (2016) and Su et al. (2017). All emissions from international shipping activities are regional nonattributable.

Table S5. Please refer to the spreadsheet in the supplementary tables, Mapping of the eleven regions. Note: The spatial mapping is based on Natural Earth data (<https://www.naturalearthdata.com>), and 1:10 m cultural vectors are applied. Columns 2 and 3 are extracted from Natural Earth maps. ADM0_A3 are the alpha-3 codes defined for each country or region.

Table S6. Equilibrium climate sensitivity (ECS) used in this study compared to other references

Model	This study	Ref [21]	Ref [22]	Ref [23]	Ref [24]	Ref [25]	Ref [26]	Ref [27]
ACCESS1-0	3.88	-	3.83	3.8	3.79	3.45	3.76	3.8
ACCESS1-3	3.59	-	-	-	3.45	2.8	3.22	-
bcc-csm1-1	2.80	-	2.82	2.8	2.88	-	2.73	2.8
bcc-csm1-1-m	2.79	-	2.87	2.9	-	-	3.1	-
BNU-ESM	4.11(*)	-	-	4.1	4.11	-	4.08	4.1
CanESM2	3.66	3.69	3.69	3.7	3.68	3.6	3.63	3.7
CCSM4	2.90	-	2.89	2.9	2.92	-	2.8	2.9
CNRM-CM5	3.27	3.25	3.25	3.3	3.25	3.16	3.07	3.3
CNRM-CM5-2	3.46	-	-	-	-	-	-	-
CSIRO-Mk3-6-0	4.24	4.08	4.08	4.1	3.99	2.96	3.55	4.1
FGOALS-g2	3.45(*)	-	-	-	3.45	-	2.46	3.45
FGOALS-s2	4.16(*)	-	4.17	-	4.16	-	4.14	4.16
GFDL-CM3	3.97	3.97	3.97	4	3.96	3.2	3.85	4
GFDL-ESM2G	2.57	2.39	2.39	2.4	2.38	-	1.81	-
GFDL-ESM2M	2.71	2.44	2.44	2.4	2.41	-	2.23	2.4
HadGEM2-ES	4.58	4.59	4.59	4.6	4.55	4.32	4.6	4.6
IPSL-CM5A-LR	4.05	4.13	4.13	4.1	4.1	3.46	3.92	4.1
IPSL-CM5A-MR	4.11	-	-	-	-	3.4	-	-
IPSL-CM5B-LR	2.64	-	2.61	2.6	2.59	-	2.43	2.6
MIROC5	2.70	2.72	2.72	2.7	2.71	2.12	2.22	2.7
MIROC-ESM	4.67	4.67	4.67	4.7	4.65	3.47	3.88	4.7
MPI-ESM-LR	3.64	3.63	3.63	3.6	3.6	3.08	3.27	-
MPI-ESM-MR	3.48	-	-	-	3.44	2.94	3.14	3.4
MPI-ESM-P	3.47	3.45	3.45	-	3.42	-	3.07	-
MRI-CGCM3	2.60	2.6	2.6	2.6	2.59	2.19	2.52	2.6
NorESM1-M	2.82	2.8	2.8	2.8	2.83	2.11	2.48	2.8

(*) The ECS values for BNU-ESM, FGOALS-g2 and FGOALS-s2 are retrieved from ref [24]. All other values in this study are estimated by using the standard regression method [22, 28] based on the available CMIP5 experiments of the preindustrial control (piControl) and abrupt 4xCO₂ scenario (abrupt4xCO₂). (**) Based on Table 9.5 in IPCC AR5-WG1 [23].

Table S7. Please refer to the spreadsheet in the supplementary tables, Sector mapping. Note:

(*) The AIM/CGE negative CO₂ and land-use CO₂ emissions are extracted from the regional dataset rather than from the spatial dataset. (**) Forest burning and grassland burning levels are adjusted based on the percentage share in 2012 in EDGAR v4.3.2.

Table S8. An overview of the iterations regarding the climate system, scenarios, regions, sectors and emissions

Sources	Quantity	Composition
Climate system	63	Terrestrial carbon cycle, ocean carbon cycle, aerosols and pollutants, climate influences, cloud effects, climate system
Scenarios	7	1.9 Wm ⁻² , 2.6 Wm ⁻² , 3.4 Wm ⁻² , 4.5 Wm ⁻² , 6.0 Wm ⁻² , 7.0 Wm ⁻² and 8.5 Wm ⁻²
Regions	11	CHN, IND, JPN, RUS, USA, AFR, EUR, LAM, MEA, OAS, ROW
Sectors	12	Agriculture, agricultural waste burning, domestic housing and commercial, energy, industry, industrial solvents, surface transportation, waste treatment, open forest burning, open grassland burning, aviation and international shipping
Emissions	48	Industrial CO ₂ , land-use CO ₂ , CH ₄ , N ₂ O, BC, CO, NH ₃ , NO _x , OC, SO ₂ , VOCs and halogenated gases (a total of 37 gases including HFC-23, HFC-32, HFC-125, HFC-134a, HFC-143a, HFC-152a, HFC-227ea, HFC-236fa, HFC-245fa, HFC-365mfc, HFC-43-10mee, CF ₄ , C ₂ F ₆ , C ₃ F ₈ , c-C ₄ F ₈ , C ₄ F ₁₀ , C ₅ F ₁₂ , C ₆ F ₁₄ , C ₇ F ₁₆ ; SF ₆ , NF ₃ , CFC-11, CFC-12, CFC-113, CFC-114, CFC-115, CCl ₄ , CH ₃ CCl ₃ , HCFC-22, HCFC-141b, HCFC-142b, Halon-1211, Halon-1202, Halon-1301, Halon-2402, CH ₃ Br and CH ₃ Cl)

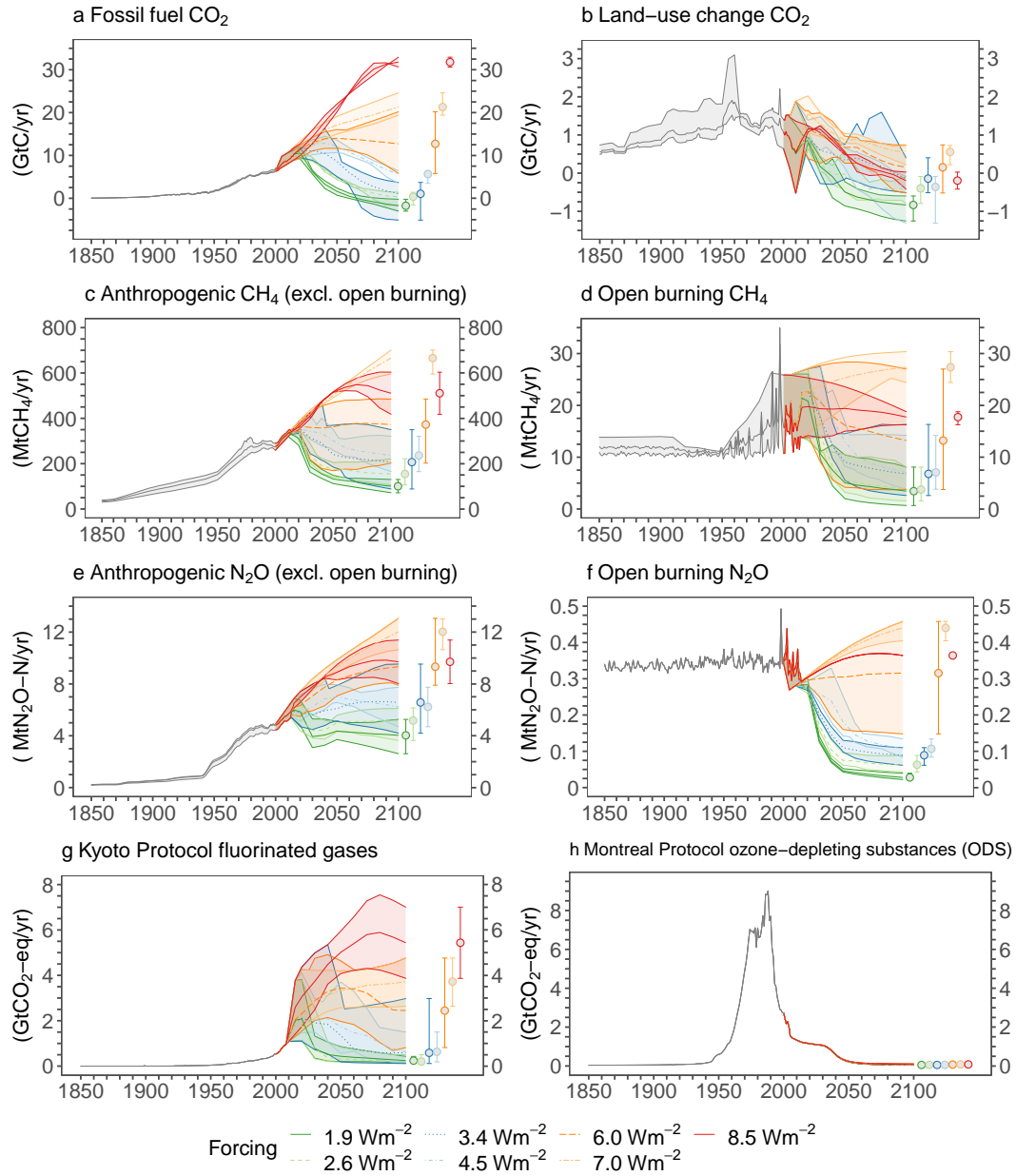


Figure S1. Historical and future GHG emissions. The future projections include seven forcing levels, namely, 1.9 Wm⁻², 2.6 Wm⁻², 3.4 Wm⁻², 4.5 Wm⁻², 6.0 Wm⁻², 7.0 Wm⁻² and 8.5 Wm⁻². The uncertainty ranges denote the upper and lower trends. The error bars to the right show the upper and lower trends in 2100 at each forcing level. Open burning includes the emissions from agricultural waste burning, forest fires and grassland fires. Sources: the historical emissions stem from ref [10, 11, 13, 14]; the future trends stem from ref [15, 16]; land-use CO₂ originates from ref [13, 19, 20, 29]; open burning is from ref [30].

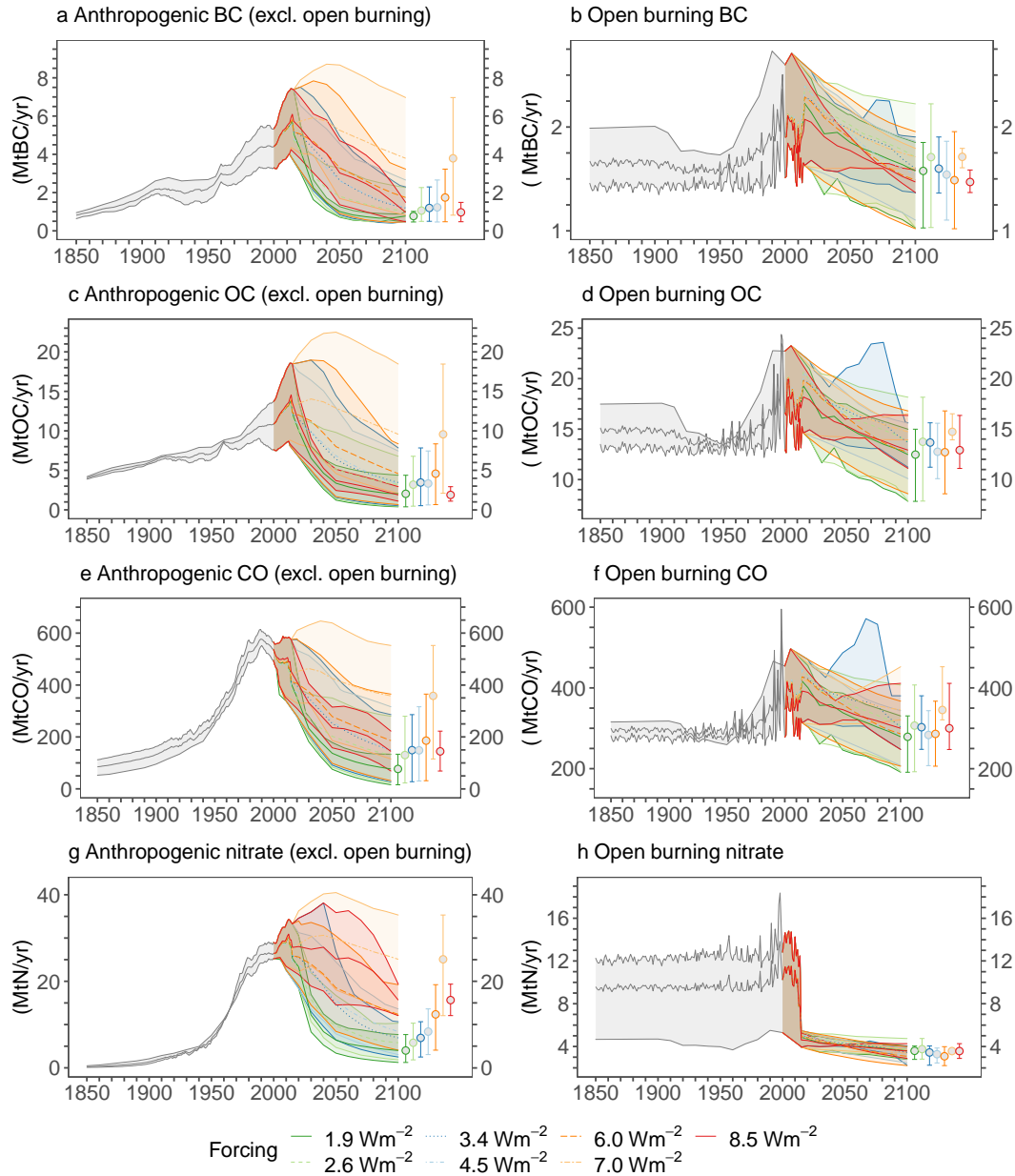


Figure S2. Historical and future aerosol and pollutant emissions (a-h). The future projections include seven forcing levels, namely, 1.9 Wm⁻², 2.6 Wm⁻², 3.4 Wm⁻², 4.5 Wm⁻², 6.0 Wm⁻², 7.0 Wm⁻² and 8.5 Wm⁻². The uncertainty ranges denote the upper and lower trends. The error bars to the right show the upper and lower trends in 2100 at each forcing level. Open burning includes the emissions from agricultural waste burning, forest fires and grassland fires. Sources: the historical emissions stem from ref [10, 11, 13, 14]; future trends come from ref [15, 16]; open burning originates from ref [30].

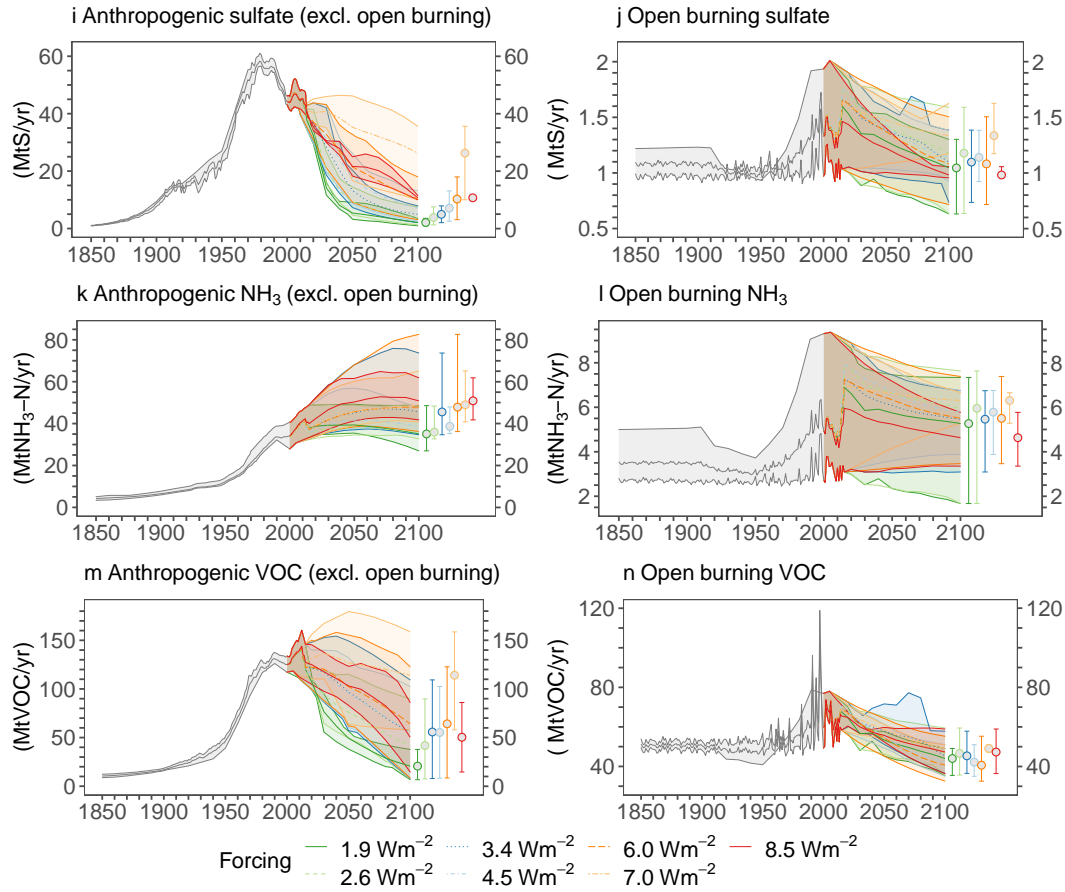


Figure S3. Historical and future aerosol and pollutant emissions (i-n). The future projections include seven forcing levels, namely, 1.9 Wm⁻², 2.6 Wm⁻², 3.4 Wm⁻², 4.5 Wm⁻², 6.0 Wm⁻², 7.0 Wm⁻² and 8.5 Wm⁻². The uncertainty ranges denote the upper and lower trends. The error bars to the right show the upper and lower trends in 2100 at each forcing level. Open burning includes the emissions from agricultural waste burning, forest fires and grassland fires. Sources: the historical emissions are from ref [10, 11, 13, 14]; future trends come from ref [15, 16]; open burning stems from ref [30].

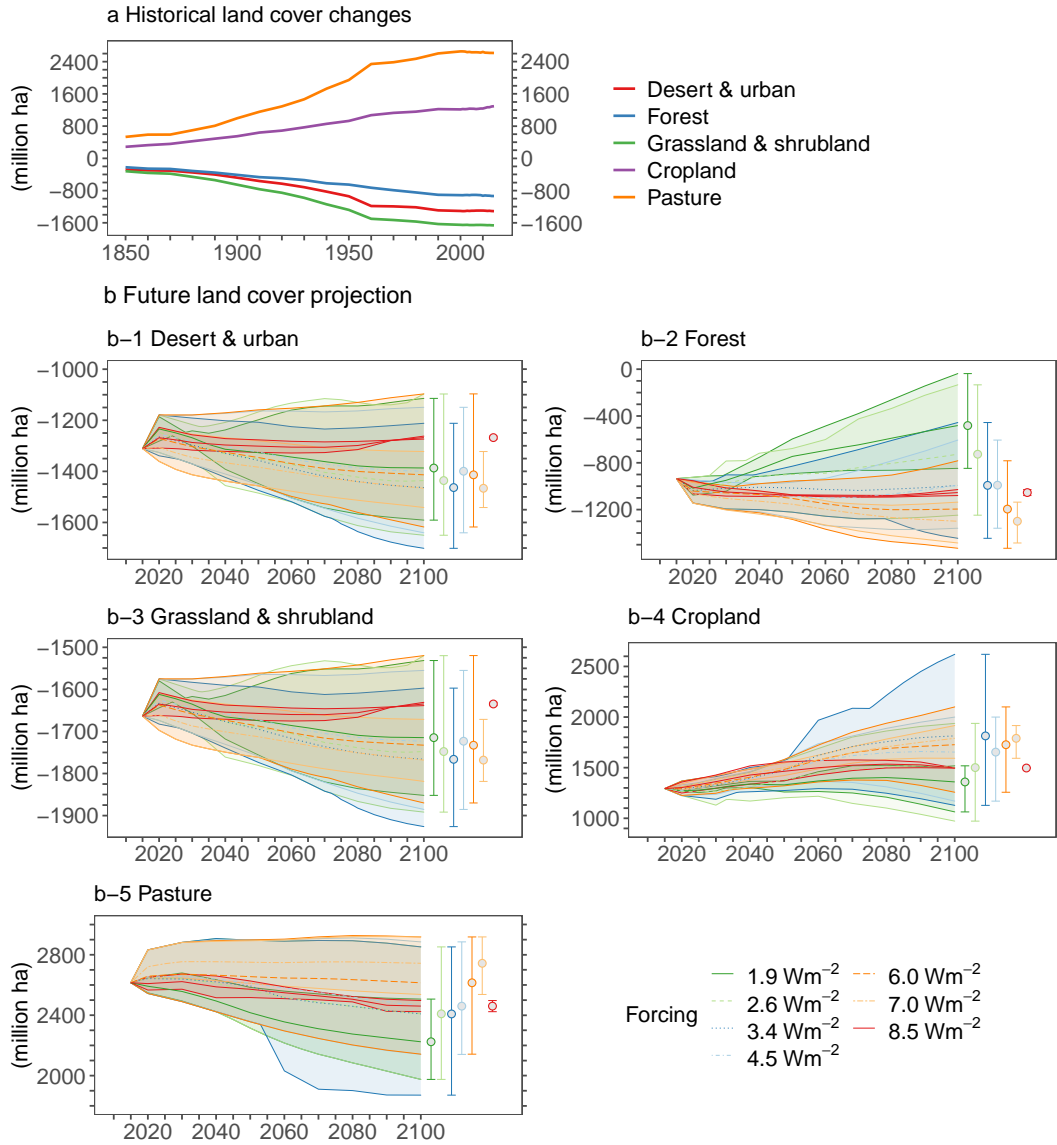


Figure S4. Historical and future land cover changes, compared to the values in 1700. The future projections include seven forcing levels, namely, 1.9 Wm⁻², 2.6 Wm⁻², 3.4 Wm⁻², 4.5 Wm⁻², 6.0 Wm⁻², 7.0 Wm⁻² and 8.5 Wm⁻². The uncertainty ranges denote the upper and lower trends. The error bars to the right show the upper and lower trends in 2100 at each forcing level. Sources: LUH2 v2h [31]; LUH2 v2f [32]; AIM-SSP/RCP gridded emission and land-use data [15].

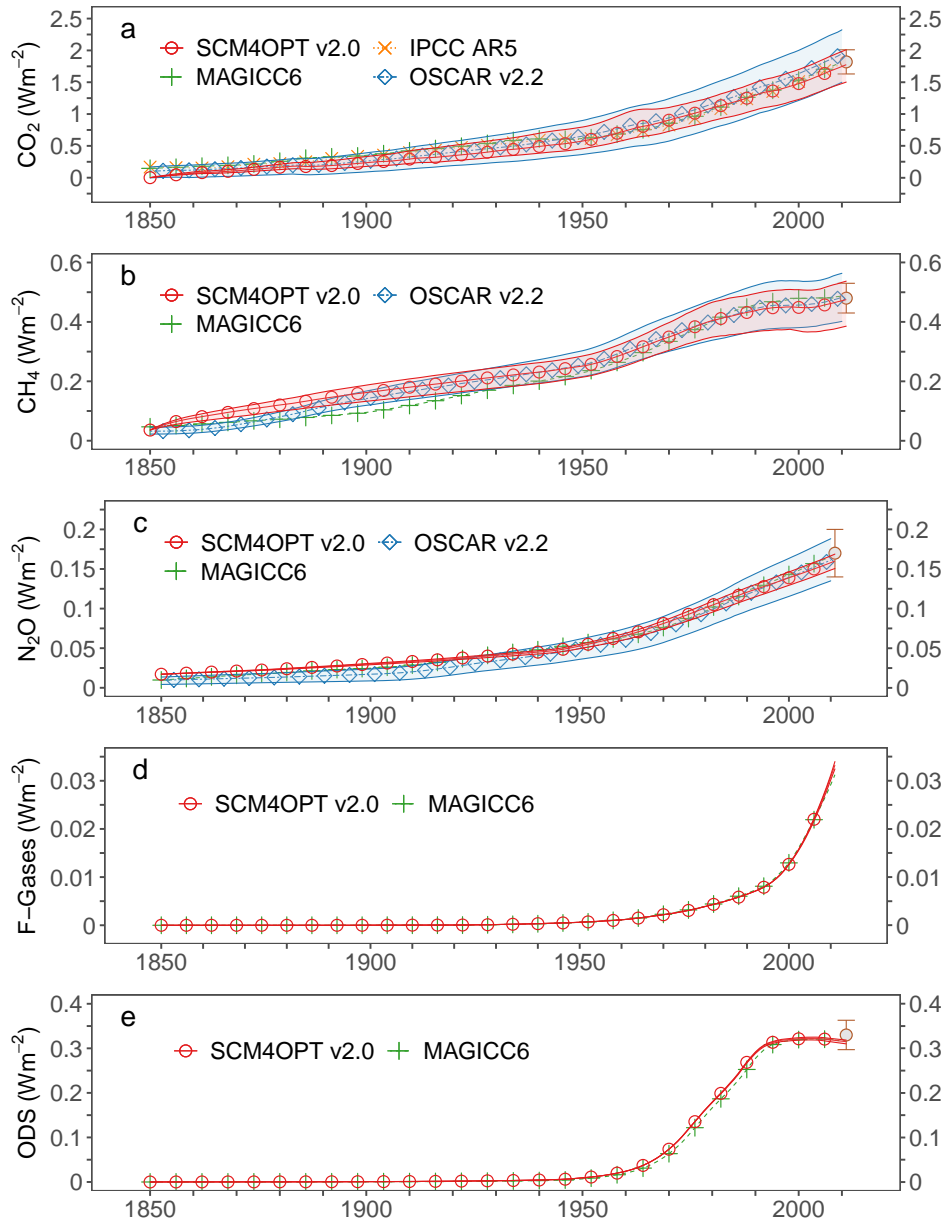


Figure S5. Simulation of the radiative forcings induced by greenhouse gases (GHGs) compared to existing studies (IPCC AR5 [33], MAGICC6 [4] and OSCAR v2.2 [5]). The uncertainties in SCM4OPT v2.0 indicate the 17th and 83rd percentiles. The MAGICC6 time series are extracted from RCP calculations [34]. The OSCAR v2.2 uncertainties are produced by 500 runs, accounting for the 17th and 83rd percentiles, downloaded from <https://github.com/tgasser/OSCARv2>. The error bars in 2011 denote the forcing values over the period of 1750-2011 in IPCC AR5 (Table 8.2).

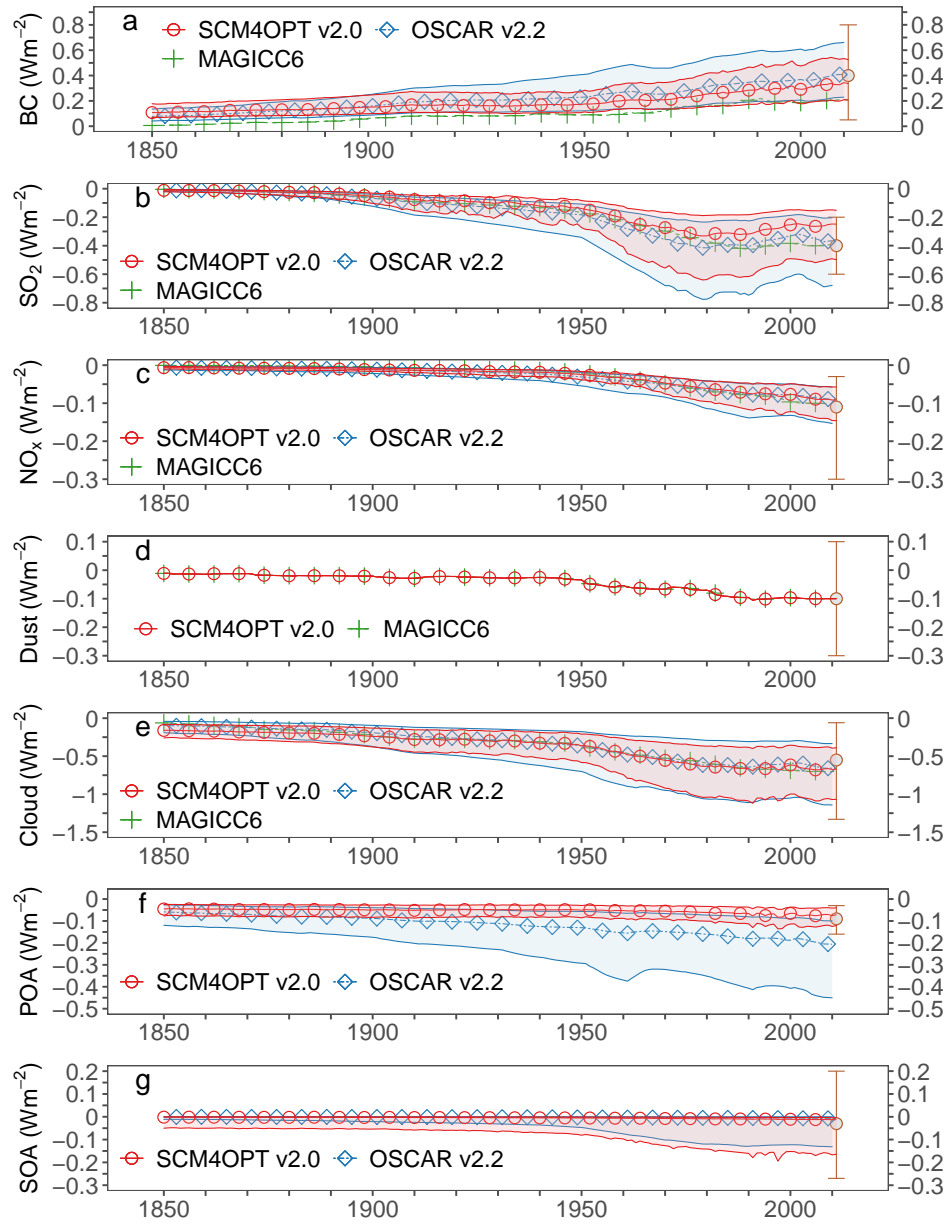


Figure S6. Simulation of the radiative forcings induced by aerosols and pollutants, compared to existing studies (IPCC AR5 [33, 35], MAGICC6 [4] and OSCAR v2.2 [5]). The uncertainties in SCM4OPT v2.0 indicate the 17th and 83rd percentiles. The MAGICC6 time series are extracted from RCP calculations [34]. The OSCAR v2.2 uncertainties are produced by 500 runs, accounting for the 17th and 83rd percentiles. The error bars in 2011 denote the forcing values over the period of 1750-2011 in IPCC AR5 (Table 8.4 and Figure SPM.5).

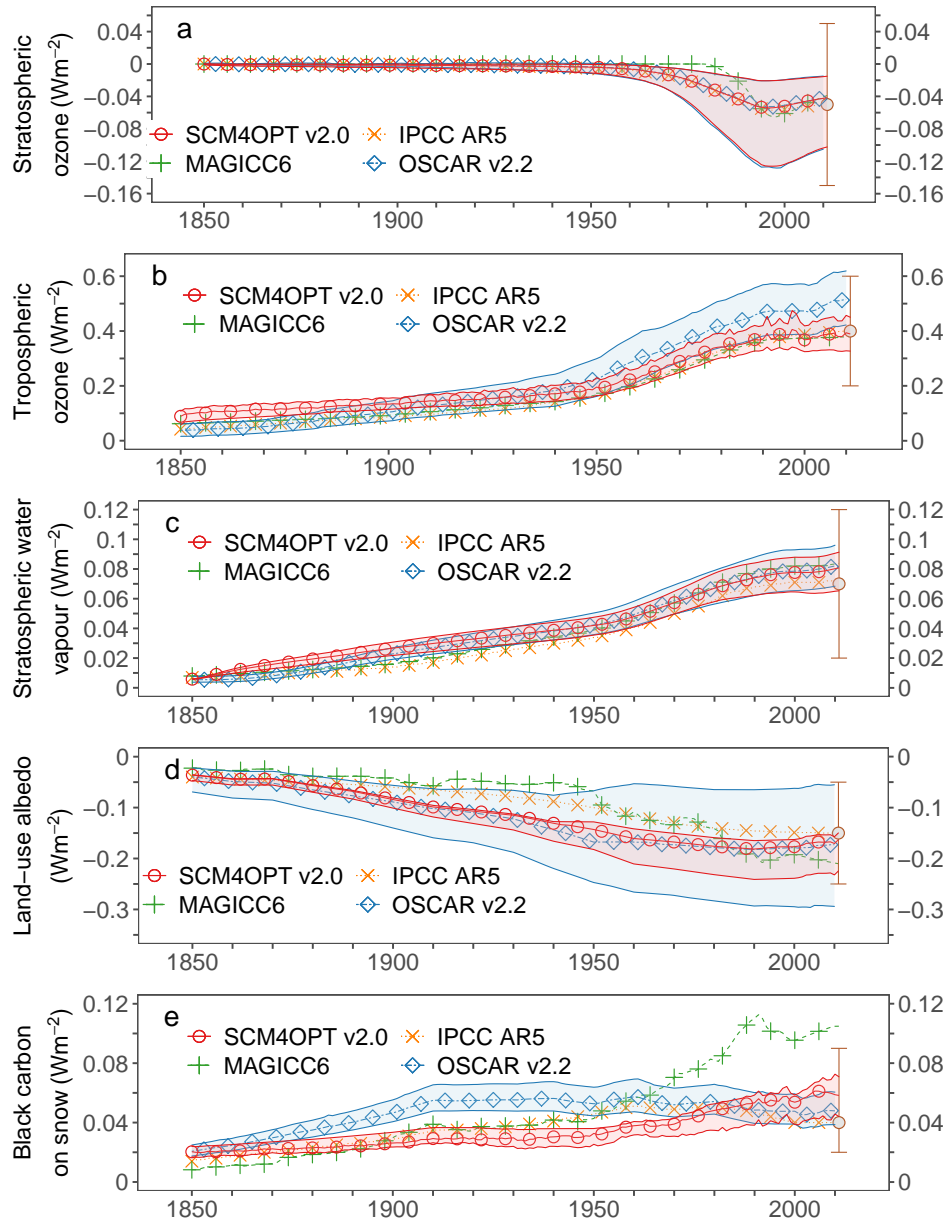


Figure S7. Simulation of the radiative forcings induced by human activities, other than the GHGs and aerosols and pollutants above, compared to existing studies (IPCC AR5 [33], MAGICC6 [4] and OSCAR v2.2 [5]). The uncertainties in SCM4OPT v2.0 indicate the 17th and 83rd percentiles. The MAGICC6 time series are extracted from RCP calculations [34]. The OSCAR v2.2 uncertainties are produced by 500 runs, accounting for the 17th and 83rd percentiles. The error bars in 2011 denote the forcing values over the period of 1750-2011 in IPCC AR5 (Table 8.6).

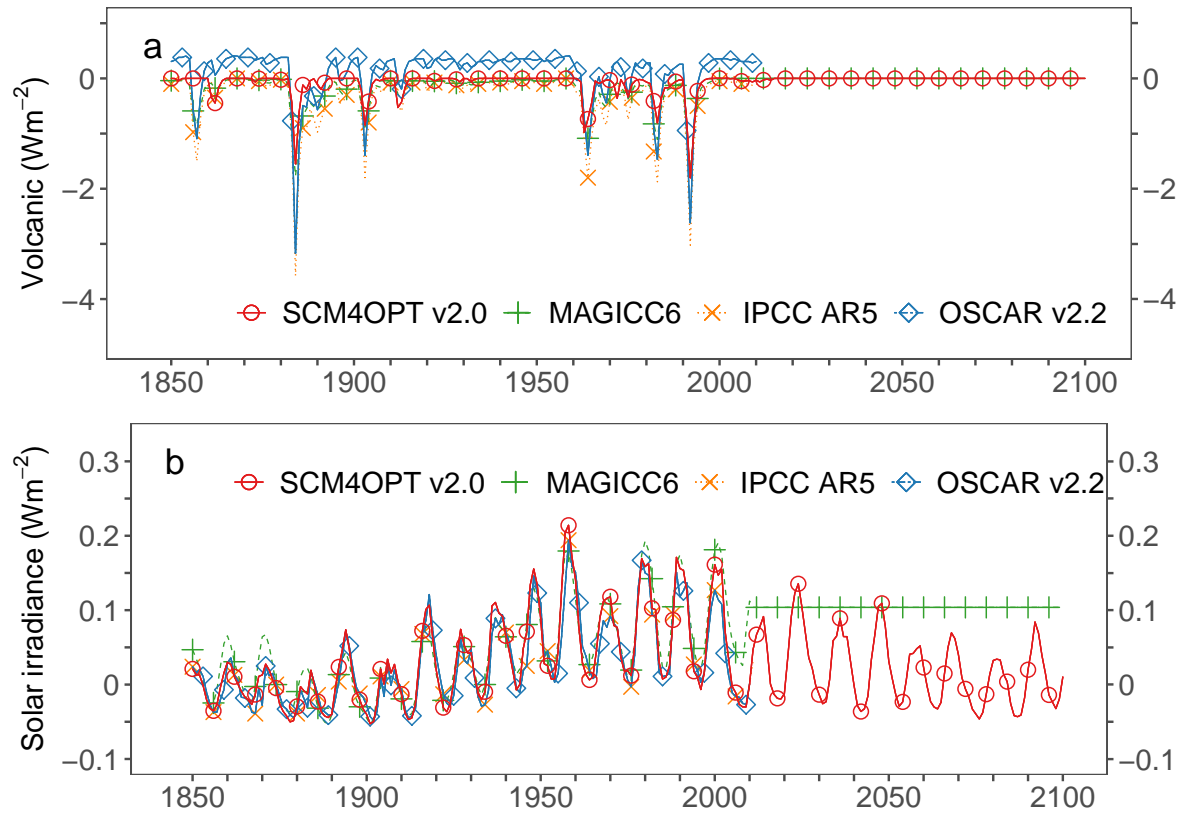


Figure S8. Assumptions of the radiative forcings induced by the natural sources of volcanic activity and solar irradiance compared to existing studies. The volcanic and solar irradiance forcings used in SCM4OPT v2.0 are assumed in accordance with volcanic activity [36] and solar irradiance [37] forcing inputs for CMIP6, and the volcanic forcing is normalized to zero in 1850.

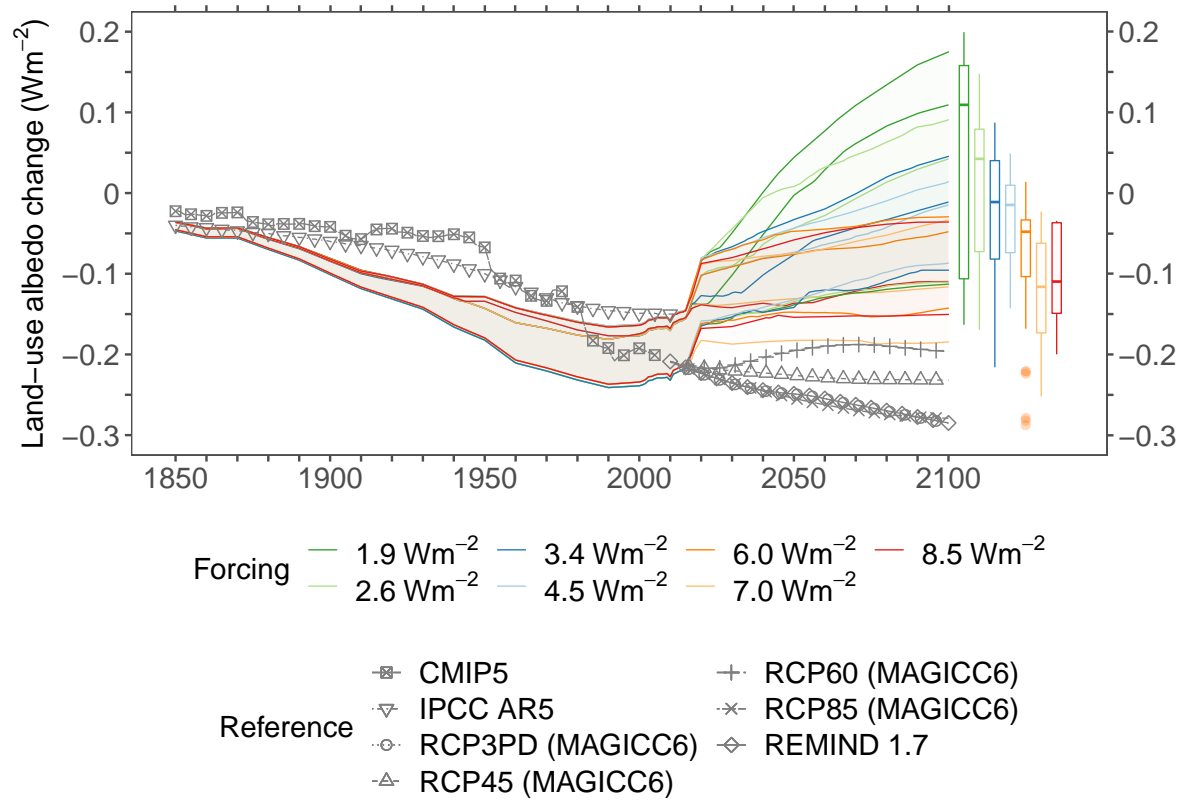


Figure S9. Land-use albedo forcings estimated by SCM4OPT v2.0 compared to existing studies. REMIND 1.7 uses default exogenous values as the future outlook (extracted from the source code, <https://www.pik-potsdam.de/research/transformation-pathways/models/remind>). The RCP scenarios are produced by MAGICC6 [34]. The uncertainties in SCM4OPT v2.0 indicate the 17th and 83rd percentiles. The boxplot to the right shows the distributions in 2100, with the upper and lower hinges corresponding to the 25th and 75th percentiles, respectively, where the upper whisker denotes 1.5 times the interquartile range above the 75th percentile, and the lower whisker denotes 1.5 times the interquartile range below the 25th percentile.

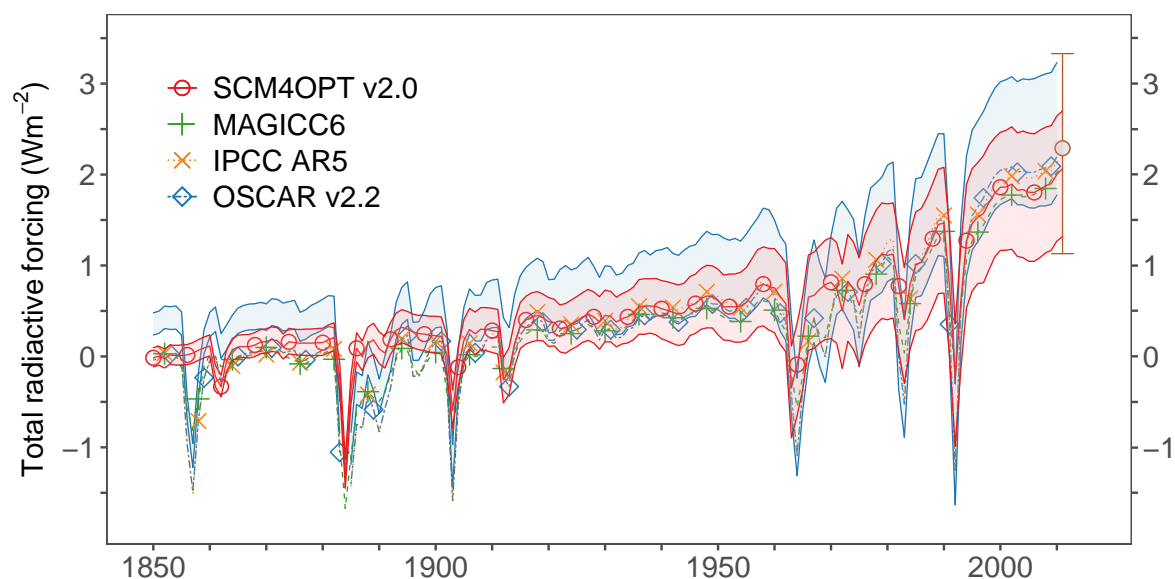


Figure S10. Total radiative forcing simulated by SCM4OPT v2.0 compared to existing studies (IPCC AR5 [33], MAGICC6 [4] and OSCAR v2.2 [5]). The uncertainties in SCM4OPT v2.0 indicate the 17th and 83rd percentiles. The MAGICC6 time series are extracted from RCP calculations [34]. The OSCAR v2.2 uncertainties are produced by 500 runs, accounting for the 17th and 83rd percentiles. The error bars in 2011 denote the total anthropogenic radiative forcing relative to 1750 (Figure SPM.5).

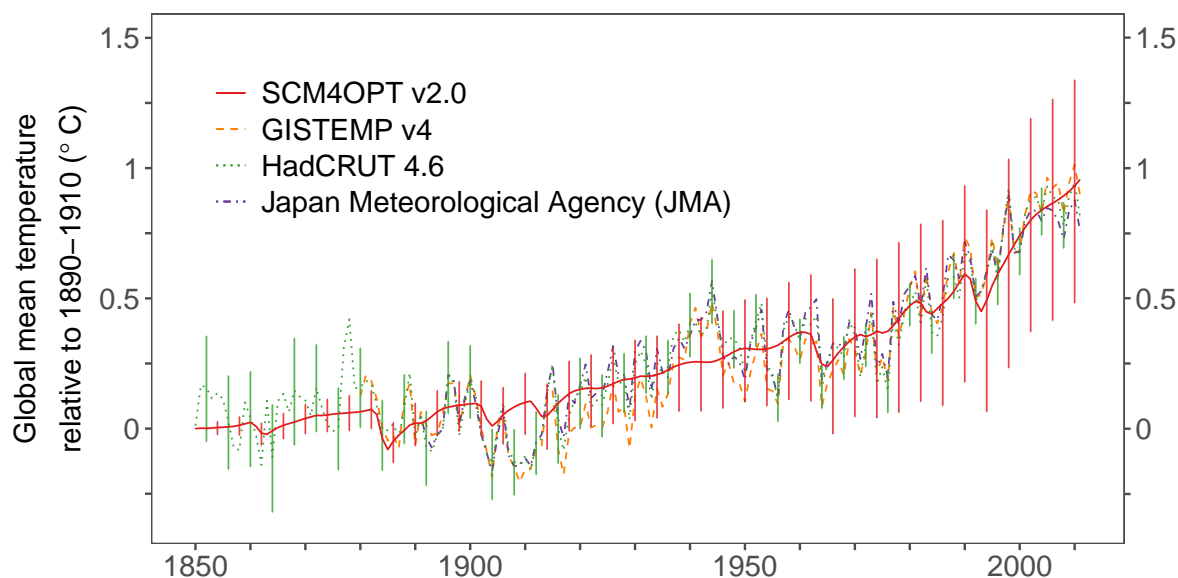


Figure S11. Historical global mean temperature increase above the preindustrial level, generated by SCM4OPT v2.0 and compared to existing statistical records. The anomalies deviate from the average over 1890–1910. The SCM4OPT v2.0 uncertainties result from the emission source- (CEDS [10], EDGAR v4.3.2 [11] and RCP historical [34]) and climate uncertainties described in this paper. The uncertainties in HadCRUT 4.6 indicate the 95% confidence interval of the combined effects of all the uncertainties described in the HadCRUT4 error model. GISTEMP v4 from ref [38]; HadCRUT 4.6 from ref [39]; Japan Meteorological Agency (JMA) from ref [40].

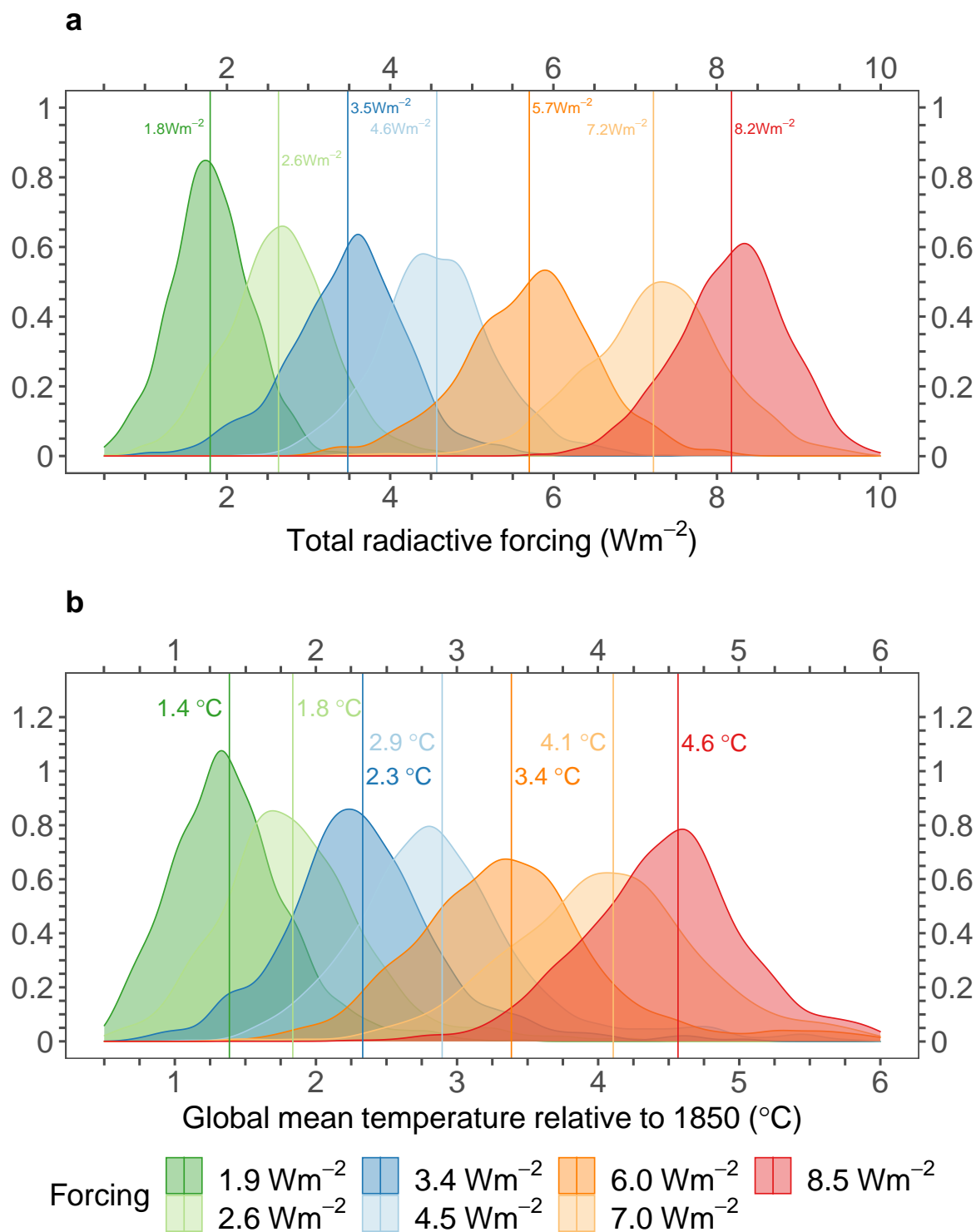


Figure S12. Probability distributions of the total radiative forcing and global mean temperature at forcing levels of 1.9 Wm⁻², 2.6 Wm⁻², 3.4 Wm⁻², 4.5 Wm⁻², 6.0 Wm⁻², 7.0 Wm⁻² and 8.5 Wm⁻², estimated by SCM4OPT v2.0. a, Total radiative forcing in 2100. b, Global mean temperature increase relative to 1850 in 2100. The color values indicate the mean value at each forcing level.

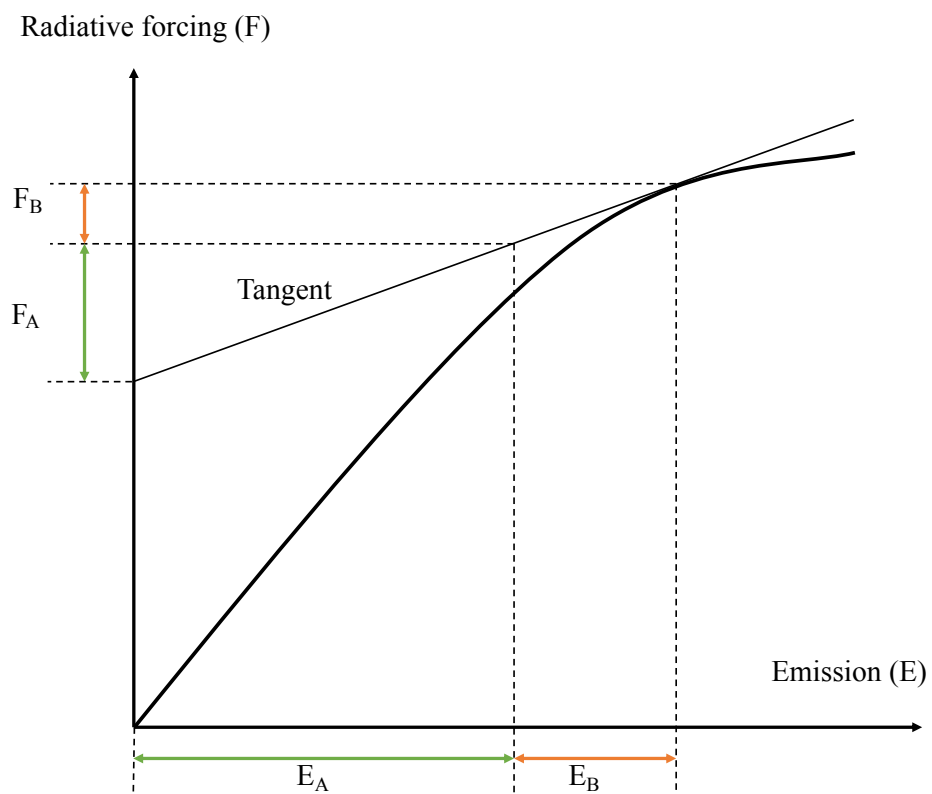


Figure S13. The normalized marginal method for the attributions of radiative forcings.
The figure is plotted based on Figure 5 in ref [41].

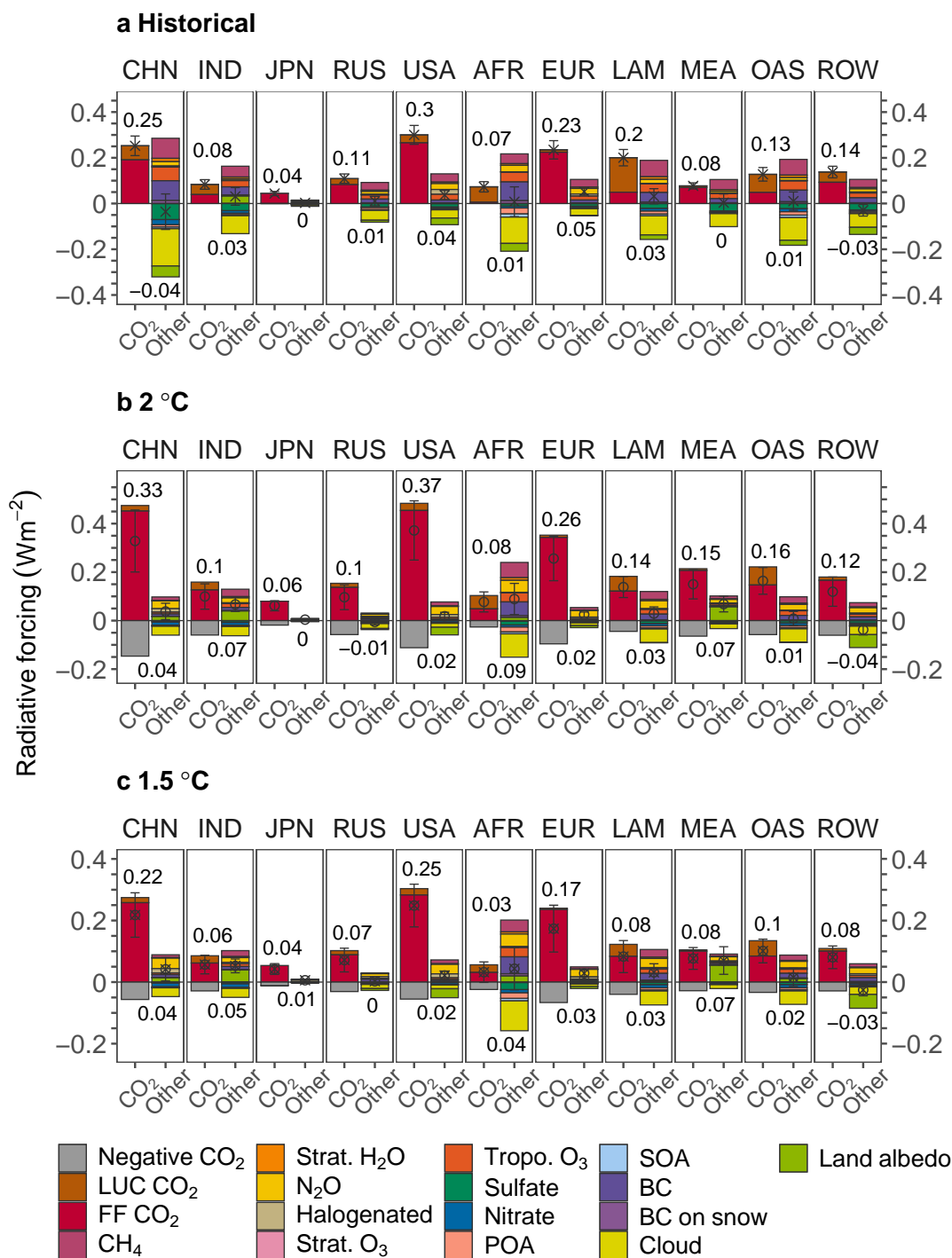


Figure S14. Regional forcings are decomposed into CO₂-induced forcings and those not directly related to CO₂. a, Historical period (1850-2016); b, 2 °C (1850-2100); c, 1.5 °C (1850-2100). The direct CO₂ emissions are separated into fossil-fuel CO₂ (FF CO₂), land-use CO₂ (LUC CO₂), and negative CO₂ emissions, if applicable. The value on top of the bar indicates the mean value summing all components of the left CO₂ bar. The value at the bottom of the bar indicates the mean value summing all components of the right bar. All uncertainties are represented as one standard deviation.

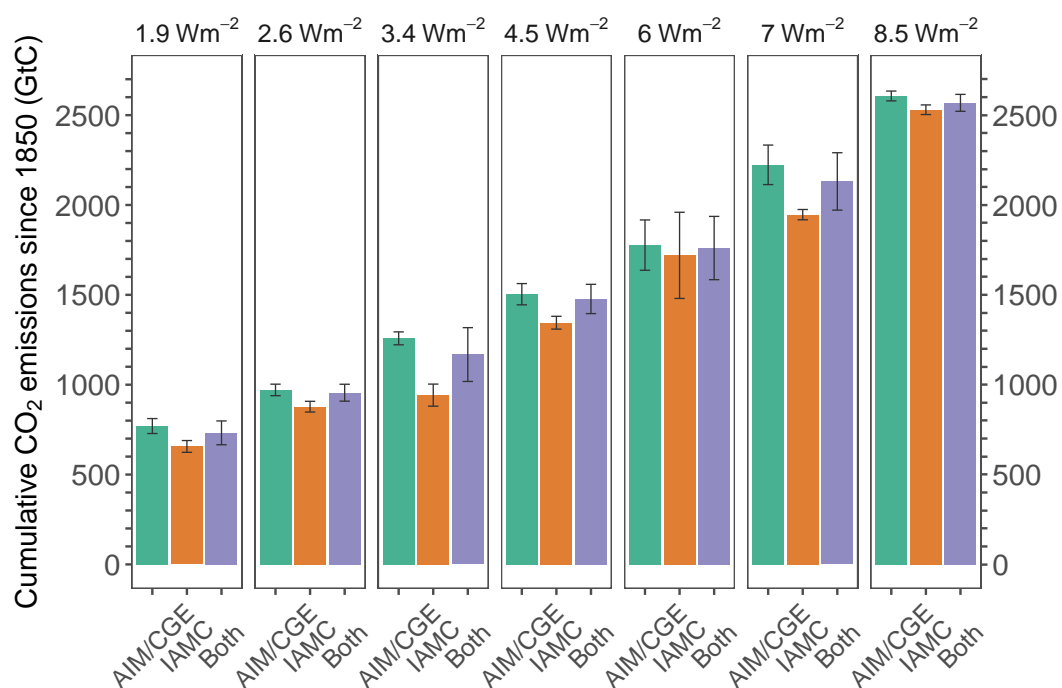


Figure S15. Cumulative CO₂ emissions projected by AIM/CGE and IAMC. The uncertainties are represented as one standard deviation. All the AIM/CGE projections are slightly higher than those by the IAMC. This figure shows only the cumulative CO₂ emissions, representing part of the systematic deviations, and variations regarding aerosols and pollutants also occur.

- [1] Hartin C A, Patel P, Schwarber A, Link R P and Bond-Lamberty B P 2015 *Geoscientific Model Development* **8** 939–955
- [2] Hartin C A, Bond-Lamberty B, Patel P and Mundra A 2016 *Biogeosciences* **13** 4329–4342
- [3] Ramaswamy V, Boucher O, Haigh J, Hauglustaine D, Haywood J, Myhre G, Nakajima T, Shi G and Solomon S 2002 *Radiative Forcing of Climate Change* (Cambridge, United Kingdom and New York, NY, USA: Cambridge University Press) chap 6, pp 349–416
- [4] Meinshausen M, Raper S C B and Wigley T M L 2011 *Atmospheric Chemistry and Physics* **11** 1417–1456
- [5] Gasser T, Ciais P, Boucher O, Quilcaille Y, Tortora M, Bopp L and Hauglustaine D 2017 *Geoscientific Model Development* **10** 271–319
- [6] Tanaka K and Kriegler E 2007 Aggregated Carbon cycle, atmospheric chemistry and climate model (ACC2): description of forward and inverse mode Tech. rep. Max Planck Institute for Meteorology
- [7] Wong T E, Bakker A M R, Ruckert K, Applegate P, Slangen A B A and Keller K 2017 *Geoscientific Model Development* **10** 2741–2760
- [8] Myhre G, Highwood E J, Shine K P and Stordal F 1998 *Geophysical Research Letters* **25** 2715–2718
- [9] Gifford R M 1993 *Implications of CO₂ Effects on Vegetation for the Global Carbon Budget* (Berlin, Heidelberg: Springer Berlin Heidelberg) pp 159–199 ISBN 978-3-642-84608-3
- [10] Hoesly R M, Smith S J, Feng L, Klimont Z, Janssens-Maenhout G, Pitkanen T, Seibert J J, Vu L, Andres R J, Bolt R M, Bond T C, Dawidowski L, Kholod N, Kurokawa J I, Li M, Liu L, Lu Z, Moura M C P, O'Rourke P R and Zhang Q 2018 *Geoscientific Model Development* **11** 369–408
- [11] Aardenne J A V, Monni S, Doering U, Olivier J G J and Pagliari V 2018 *Earth System Science Data* **10** 1987–2013
- [12] JRC and PBL 2011 Global Emissions EDGAR v4.2 (November 2011)
- [13] Gütschow J, Jeffery M L, Gieseke R, Gebel R, Stevens D, Krapp M and Rocha M 2016 *Earth System Science Data* **8** 571–603
- [14] Lamarque J F, Smith S J, Bond T, Cofala J, Eyring V, Granier C, Heil A, Kainuma M, Klimont Z, Lee D, Liousse C, Mieville A, Riahi K, Schultz M, Stevenson D, Aardenne J V and van Vuuren D 2009 Historical emissions data (1850 - 2000)
- [15] Fujimori S, Hasegawa T, Ito A, Takahashi K and Masui T 2018 *Scientific Data* **5** 1–13
- [16] Gidden M J, Riahi K, Smith S J, Fujimori S, Luderer G, Kriegler E, Van Vuuren D P, Van Den Berg M, Feng L, Klein D, Calvin K, Doelman J C, Frank S, Fricko O, Harmsen M, Hasegawa T, Havlik P, Hilaire J, Hoesly R, Horing J, Popp A, Stehfest E and Takahashi K 2019 *Geoscientific Model Development* **12** 1443–1475
- [17] Houghton R A, House J I, Pongratz J, van der Werf G R, DeFries R S, Hansen M C, Le Quéré C and Ramankutty N 2012 *Biogeosciences* **9** 5125–5142
- [18] Hansis E, Davis S J and Pongratz J 2015 *Global Biogeochemical Cycles* **29** 1230–1246
- [19] Raddatz T 2010 Historical landcover change and wood harvest CO₂ emissions
- [20] Smith S J and Rothwell A 2013 *Biogeosciences* **10** 6323–6337
- [21] Andrews T, Gregory J M, Webb M J and Taylor K E *Geophysical Research Letters* **39**
- [22] Forster P M, Andrews T, Good P, Gregory J M, Jackson L S and Zelinka M 2013 *Journal of Geophysical Research: Atmospheres* **118** 1139–1150
- [23] IPCC 2014 *Climate Change 2014: Synthesis Report. Contribution of Working Groups I, II and III to the Fifth Assessment Report of the Intergovernmental Panel on Climate Change* ISBN 9789291691432
- [24] Sherwood S C, Bony S and Dufresne J L 2014 *Nature* **505** 37–42
- [25] Gregory J M, Andrews T and Good P 2015 *Philosophical Transactions of the Royal Society of London A: Mathematical, Physical and Engineering Sciences* **373**
- [26] Tsutsui J 2017 *Climatic Change* **140** 287–305
- [27] Mauritzen C, Zivkovic T and Veldore V 2017 *Tellus Series a-Dynamic Meteorology and Oceanography* **69** 1–12
- [28] Gregory J M, Ingram W J, Palmer M A, Jones G S, Stott P A, Thorpe R B, Lowe J A, Johns T C and Williams K D 2004 *Geophysical Research Letters* **31**
- [29] Le Quéré C, Andrew R M, Friedlingstein P, Sitch S, Hauck J, Pongratz J, Pickers P A, Korsbakken J I,

- Peters G P, Canadell J G, Arneth A, Arora V K, Barbero L, Bastos A, Bopp L, Chevallier F, Chini L P, Ciais P, Doney S C, Gkritzalis T, Goll D S, Harris I, Haverd V, Hoffman F M, Hoppema M, Houghton R A, Hurtt G, Ilyina T, Jain A K, Johannessen T, Jones C D, Kato E, Keeling R F, Goldewijk K K, Landschützer P, Lefèvre N, Lienert S, Liu Z, Lombardozzi D, Metzl N, Munro D R, Nabel J E M S, Nakaoka S I, Neill C, Olsen A, Ono T, Patra P, Peregon A, Peters W, Peylin P, Pfeil B, Pierrot D, Poulter B, Rehder G, Resplandy L, Robertson E, Rocher M, Rödenbeck C, Schuster U, Schwinger J, Séférian R, Skjelvan I, Steinhoff T, Sutton A, Tans P P, Tian H, Tilbrook B, Tubiello F N, van der Laan-Luijkx I T, van der Werf G R, Viovy N, Walker A P, Wiltshire A J, Wright R, Zaehle S and Zheng B 2018 *Earth System Science Data* **10** 2141–2194
- [30] van Marle M J E, Kloster S, Magi B I, Marlon J R, Daniaou A L, Field R D, Arneth A, Forrest M, Hantson S, Kehrwald N M, Knorr W, Lasslop G, Li F, Mangeon S, Yue C, Kaiser J W and van der Werf G R 2017 *Geoscientific Model Development* **10** 3329–3357
- [31] Hurtt G, Chini L, Frolking S and Sahajpal R 2016 Land-Use Harmonization (LUH2) - LUH2 v2h
- [32] Hurtt G, Chini L, Sahajpal R, Frolking S and et al 2016 Land-Use Harmonization (LUH2) - LUH2 v2f
- [33] Myhre G, Shindell D, Breon F M, Collins W, Fuglestad J, Huang J, Koch D, Lamarque J F, Lee D, Mendoza B, Nakajima T, Robock A, Stephens G, Takemura T and Zhang H 2013 *Anthropogenic and Natural Radiative Forcing* (Cambridge, United Kingdom and New York, NY, USA: Cambridge University Press) book section 8, pp 659–740 ISBN ISBN 978-1-107-66182-0
- [34] Meinshausen M, Smith S J, Calvin K, Daniel J S, Kainuma M L T, Lamarque J F, Matsumoto K, Montzka S A, Raper S C B, Riahi K, Thomson A, Velders G J M and van Vuuren D P 2011 *Climatic Change* **109** 213–241
- [35] IPCC 2013 *Summary for Policymakers* (Cambridge, United Kingdom and New York, NY, USA: Cambridge University Press) book section SPM, pp 1–30 ISBN ISBN 978-1-107-66182-0
- [36] Zanchettin D, Khodri M, Timmreck C, Toohey M, Schmidt A, Gerber E P, Hegerl G, Robock A, Pausata F S, Ball W T, Bauer S E, Bekki S, Dhomse S S, Le Grande A N, Mann G W, Marshall L, Mills M, Marchand M, Niemeier U, Poulain V, Rozanov E, Rubino A, Stenke A, Tsigaridis K and Tummon F 2016 *Geoscientific Model Development* **9** 2701–2719
- [37] Matthes K, Funke B, Andersson M E, Barnard L, Beer J, Charbonneau P, Clilverd M A, Dudok de Wit T, Haberleiter M, Hendry A, Jackman C H, Kretschmar M, Kruschke T, Kunze M, Langematz U, Marsh D R, Maycock A C, Misios S, Rodger C J, Scaife A A, Seppälä A, Shangguan M, Sinnhuber M, Tourpali K, Usoskin I, van de Kamp M, Verronen P T and Versick S 2017 *Geoscientific Model Development* **10** 2247–2302
- [38] Team G 2019 GISS Surface Temperature Analysis (GISTEMP), version 4
- [39] Morice C P, Kennedy J J, Rayner N A and Jones P D 2012 *Journal of Geophysical Research: Atmospheres* **117**
- [40] (JMA) J M A 2019 Annual Anomalies of Global Average Surface Temperature (° C)
- [41] UNFCCC 2002 Methodological Issues: Scientific and Methodological Assessment of Contributions to Climate Change, Report of the Expert Meeting, Note by the Secretariat Tech. rep. URL <https://unfccc.int/resource/docs/2002/sbsta/inf14.pdf>